

# UC Berkeley

## UC Berkeley Previously Published Works

### Title

Analysis of countercurrent membrane vapor extraction of a dilute aqueous biosolute

### Permalink

<https://escholarship.org/uc/item/4z99x0pn>

### Journal

AIChE Journal, 61(9)

### ISSN

0001-1541

### Authors

Liu, David E  
Cerretani, Colin  
Tellez, Rodrigo  
[et al.](#)

### Publication Date

2015-09-01

### DOI

10.1002/aic.14892

Peer reviewed

# Analysis of Countercurrent Membrane Vapor Extraction of a Dilute Aqueous Biosolute

David E. Liu, Colin Cerretani, Rodrigo Tellez, Agnes P. Scheer, Steve Sciamanna, Paul F. Bryan, Clayton J. Radke, and John M. Prausnitz

Dept. of Chemical and Biomolecular Engineering, University of California, Berkeley, CA 94720

DOI 10.1002/aic.14892

Published online August 7, 2015 in Wiley Online Library (wileyonlinelibrary.com)

*Removal of dilute bioproducts from fermenter broths is a major challenge both to avoid microbe inhibition and to recover solutes economically without water loss. We analyze a proposed new process, membrane vapor extraction (MVE), where semi-volatile dilute aqueous solutes vaporize at the upstream side of an omniphobic, microporous membrane and dissolve into a nonpolar solvent highly favorable to the solutes but not to water. A new membrane-process analysis is outlined and applied to the countercurrent recovery of 2 wt % aqueous butanol by a prototype solvent (dodecane) at 40°C. Thermodynamic phase equilibria, pioneered by the Prausnitz school, are crucial to MVE process design. Over 90% of the feed butanol is recovered with essentially no water loss giving a separation factor of over 1000. Energy requirements in MVE are low. Our design calculations demonstrate that MVE is a viable separation process to remove and recover dilute aqueous biosolutes.* © 2015 American Institute of Chemical Engineers *AIChE J*, 61: 2795–2809, 2015

*Keywords:* membrane vapor extraction, phase equilibria, mass-transfer resistance, membrane convective-diffusion, separation factor, process design

## Introduction

At present, only few fuels and high-volume chemicals are produced by fermentation in large quantities; these include acetone-butanol-ethanol<sup>1,2</sup> and several organic acids.<sup>3</sup> However, dramatic advances in synthetic biology and other tools of biological engineering are currently driving a rapid expansion of this list. Potential new fermentation products of interest include propylene, butylene, butadiene, isoprene, and other light-organic building blocks<sup>4–7</sup>; hydrocarbon-fuel molecules in the boiling range of gasoline, jet fuel, and diesel<sup>8</sup>; butanol and other higher alcohols<sup>9–16</sup>; and a range of organic acids and diacids, including succinic, 3-HPA, and fatty acids or fatty esters. Each new fermentation product presents new challenges for recovery and purification.<sup>17</sup>

Water-soluble (or slightly water-soluble) biofuels and biochemicals from fermenters are typically recovered by distillation or, in some cases, by extraction followed by distillation. These recovery methods require considerable energy. Some products that are sparingly soluble in water can, in theory, be recovered by extraction and settling or centrifugation. In practice, however, emulsions strongly stabilized by cell debris and other components of fermentation broths (e.g., proteins and surfactants) often make such recovery methods problematic.

An alternate class of recovery processes for recovering volatile bioproducts from an aqueous fermentation broth is membrane distillation (MD). In MD processes, an aqueous feed stream is heated to a moderate temperature and brought into

contact with a highly hydrophobic, microporous membrane that permits only vapor transport.<sup>18–25</sup> Upon exiting the membrane at the permeate side, the feed vapor in direct-contact membrane distillation (DCMD) condenses near room temperature into an appropriate nonwetting solvent, almost always water.<sup>18–39</sup> Variants of DCMD include vacuum MD,<sup>18–25,40–44</sup> sweep-gas MD,<sup>18–25,45,46</sup> air-gap MD,<sup>18–25,47–49</sup> or membrane-gap MD.<sup>50</sup> Although desalination of high salinity brines is the main focus of MD,<sup>29,32,34–36,43,47,51</sup> a wide variety of specific applications have appeared.<sup>17–25,40,41,44,51–65</sup>

MD has the advantage of much lower operating temperatures and required vapor space than those of conventional distillation.<sup>19</sup> A disadvantage of MD, however, is low flux through the membrane; for high productivity, a large membrane surface may be required. When MD is used to recover a dilute biosolute from water, a second disadvantage of MD arises: both water and solute pass through the nonpermeative membrane. Accordingly, downstream enrichment of a dilute bioproduct requires a solute membrane flux larger than that of water in spite of considerable higher water concentration in the feed.

To overcome this second limitation, we propose an alternate membrane-based process where the permeate-receiving solvent is a nonvolatile organic liquid that presents high solubility for the solute, but does not dissolve water. Accordingly, the solvent saturates with minimal water uptake. Once water-saturation is achieved, water flux across the membrane ceases; solute enrichment is enhanced. To avoid condensation at the downstream side of the membrane, the receiving solvent is isothermal with the feed. Compared to distillation, energy consumption with membrane vapor extraction (MVE) is minimal

Correspondence concerning this article should be addressed to C. J. Radke at radke@berkeley.edu.

because enthalpies of feed vaporization and absorption by the solvent essentially cancel.

As in all membrane-based separations, the MVE process is driven by a difference in chemical potentials between the feed and solvent sides of the nonpermselective membrane, or equivalently by the difference in fugacities:  $(\gamma_i X_i P_{\text{isat}})_F - (\gamma_i X_i P_{\text{isat}})_S$ , where  $X_i$  is mole fraction of  $i$ ,  $P_{\text{isat}}$  is vapor pressure of pure liquid  $i$ , and  $\gamma_i$  is activity coefficient of  $i$ . Subscripts  $F$  and  $S$  denote the feed and solvent flow streams, respectively. As opposed to MD where  $T_F > T_S$ , in isothermal MVE,  $(P_{\text{isat}})_F = (P_{\text{isat}})_S$ ; separation is driven by a difference in component feed and solvent activities  $\gamma_i X_i$ . If  $\gamma_i$  (feed) is much larger than  $\gamma_i$  (solvent), then, even if  $X_i$  in the feed is small, it is possible to achieve isothermal separation using a nonwetting, nonselective microporous membrane. Available literature on steam-stripping demonstrates that many organic solutes (including those with vapor pressures lower than that of water) can be separated from their aqueous solutions using an isothermal chemical-potential driving force.<sup>66,67</sup>

To illustrate, suppose we wish to separate dilute butanol near its microbe-toxic concentration from an aqueous sugar solution in a fermenter. From the feed at temperature  $T$  and pressure  $P$ , we generate a vapor within the membrane pores that contains butanol and water. The vapor passes through the micropores of a nonwetting membrane where, at the pore exit, it encounters a nonvolatile solvent that “likes” butanol much more than water. The solvent (e.g., a heavy paraffinic hydrocarbon) is at the same  $T$  and  $P$  as those of the feed, which can be presaturated with water. There is no net temperature or liquid-phase pressure drop across the membrane faces and no condensation of water at the downstream side of the membrane. Depending on solvent-water solubility, however, a small amount of water may transport across the membrane and absorb into the butanol-laden solvent stream. Vapor-filled membrane pores are at a pressure lower than that of the surrounding feed and solvent liquids. The pressure difference between vapor and liquid at pore inlets and outlets is accounted for by nonwetting meniscus curvature.

We call this separation process MVE because, in effect, the downstream (receiving) solvent extracts butanol from aqueous solution. Strictly, MVE is not an MD operation because there is no applied transmembrane temperature difference. Rather, MVE more strongly resembles membrane liquid extraction (MLE).<sup>68–72</sup> Nevertheless, in all three processes, the driving force for separation remains based on phase-equilibrium differences between the upstream and downstream pore ends. An advantage of MVE over classical liquid-liquid extraction is the absence of direct liquid-liquid contact between aqueous feed and receiving solvent. Hence, MVE avoids liquid-liquid disengagement that may be difficult or undesirable due to stable emulsion formation or due to contamination of the liquid feed.

MVE also has several advantages over MLE. First, transport across the membrane occurs in the vapor phase rather than in the liquid phase. Accordingly, membrane-transport resistance for MVE is much less than that for MLE. Minimal nonvolatile solvent vapor is present in the membrane micropores to impede solute flux. Further, as the microporous-membrane pores are (relatively) large, the flux of butanol can exceed those typical of permselective membranes.<sup>17</sup>

Second, as water is essentially insoluble in the receiving solvent and as the operation is isothermal, the flux of water across the membrane is near zero. It is not exactly zero because the extracted solute may pull some water along with

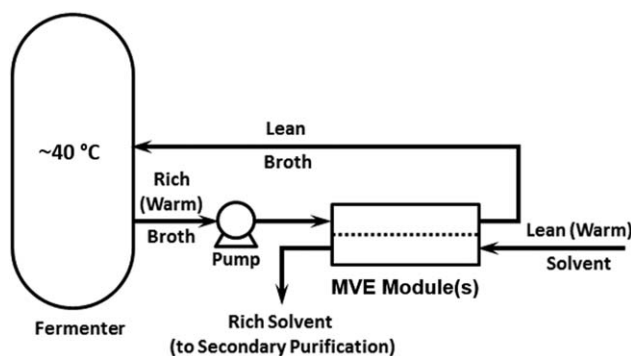


Figure 1. Schematic of the overall MVE process.

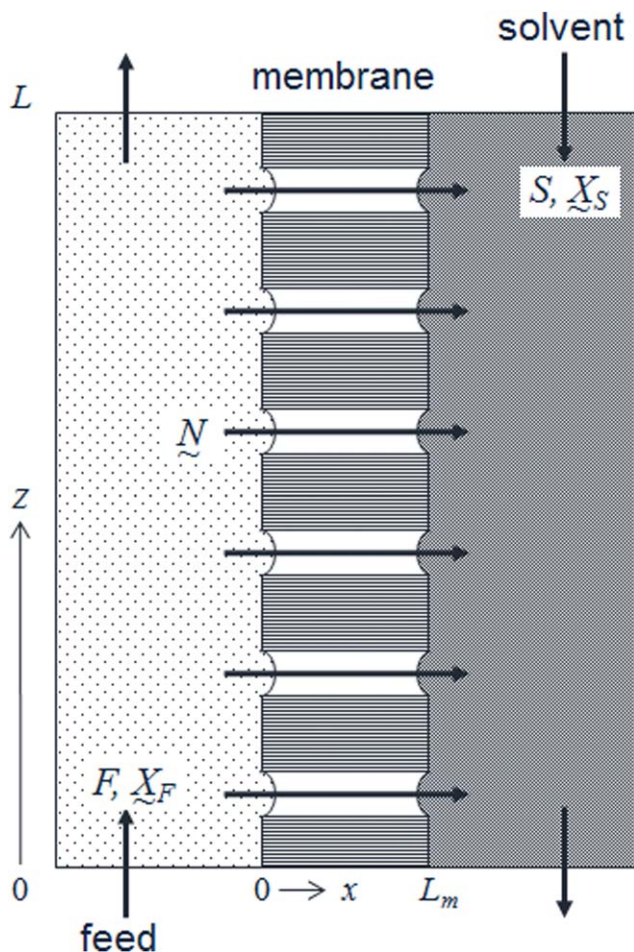
it. Third, as opposed to MD, minimal feed water is lost from the fermentation broth; make-up water for the broth is not necessary. Fourth, isothermal operation makes MVE energy efficient. And fifth, because MVE prevents liquid-liquid contact, MVE avoids formation of emulsions.

Figure 1 illustrates an MVE process to separate butanol from a dilute aqueous broth that, in a fermenter, also contains nonvolatile sugar and yeast or bacteria. Vapor from the feed solution convectively diffuses through the membrane micropores, and dissolves in the countercurrent organic solvent. Because the net flux from the feed to the solvent side is not large, concentration polarization is zero or minimal, contrary to fouling in membrane filtration. Next, a thin membrane can be used because of the small hydraulic-pressure difference between the feed and solvent sides of the membrane. Finally, the process can operate at low absolute pressure; therefore, the shell enclosing the membrane need not be a pressure vessel.

Because the volatility of butanol is several orders of magnitude larger than that of the essentially nonvolatile solvent, butanol can readily be separated from the solvent by subsequent distillation at an elevated temperature. Minimal water is lost through the MVE membrane. Thus, “entrained-particle” fouling is not likely and feed-water recovery is almost complete. These factors, coupled with improved microporous-membrane solute flux and minimal energy consumption, lead to low cost per unit of bioproduct, much lower than costs for classical liquid-liquid extraction, membrane filtration, or gas-separation modules. The MVE membrane, however, must be nonwetting both to the aqueous broth and to the organic solvent and must remain so during operation. Thus, omniphobic membranes are requisite in MVE.

Although MLE has been proposed previously,<sup>68–72</sup> to our best knowledge, MVE is new. It is analogous to pervaporation, but in MVE, the receiving phase is a liquid, not a gas. In MVE, there is no need for permeate vacuum. A liquid receiving phase eliminates the need for multiple stages of membrane separation with interstage reheating of the feed. MVE also eliminates the need to synthesize permselective membranes customized for each new application.

To date, no experimental performance data have been published for MVE. Therefore, to assess the feasibility of MVE, we present an engineering design to establish performance viability. To illustrate MVE, we consider separation of butanol from a dilute aqueous solution into dodecane at 40°C. This system is of practical importance and illustrates a case where the pure solute to be recovered is less volatile than the aqueous solvent. The chosen operating temperature of 40°C is typical of the fermentation process<sup>9,11,12,14</sup> and allows for waste-heat



**Figure 2. Schematic of countercurrent membrane vapor extraction (MVE).**

An omniphobic, microporous membrane is shown in intermediate gray shading. Components in the feed stream vaporize at the membrane, transport across the membrane, and dissolve into the solvent stream. The membrane is nonwetting to both feed and solvent streams. Feed enters with molar flow rate  $F_o$  while countercurrent solvent enters with molar flow  $S_L$ .

utilization from the bioreactor. Choice of dodecane as a prototype solvent rests primarily on the availability of pertinent vapor-liquid-liquid equilibrium data for the water/butanol/dodecane system at ambient temperature.<sup>73</sup> We present here a feasible engineering design for a countercurrent MVE module. However, later experimental verification is needed to establish a convincing proof of concept.

### MVE Design

To provide a quantitative evaluation of MVE, we present a simplified design model for the efficiency of the countercurrent separation element shown in Figure 2. An aqueous feed stream of known molar flow rate  $F$  and known mole fractions  $X_F$  (i.e., butanol at  $X_{BF}$  and water at  $X_{WF}$ ), is fed along one side of an omniphobic MD membrane. Feed butanol and some water vaporize and convectively diffuse in the  $x$  direction toward the

solvent stream with cross-membrane molar fluxes  $N$ . At  $x = L_m$ , the thickness of the membrane, the vapor dissolves into the solvent stream of molar flow rate  $S$  and mole fractions  $X_S$  (i.e., butanol at  $X_{BS}$ , water at  $X_{WS}$ , and dodecane at  $X_{DS}$ ). We assume local liquid/vapor equilibrium at the two membrane faces. Isothermal operation is imposed, although heat must be supplied to vaporize the feed stream and must be removed upon vapor dissolution in the solvent. Appendix A establishes that total thermal- and mass-transported energy transfers from the feed to the solvent. Consequently, the feed stream cools while the solvent stream warms, but each by less than tenths of degrees Celsius. Essentially isothermal operation ensues.

All flows, fluxes, and compositions vary continuously in the  $z$  direction over the length of the separation unit,  $L$ . Aqueous feed and organic solvent streams enter with known compositions,  $X_{F0}$  and  $X_{SL}$ . We focus primarily on butanol recovery and enrichment in the extract stream with composition  $X_{BS0}$  while entering in the feed stream with composition  $X_{BF0}$ . Minimal water loss in the raffinate is also an important design criterion.

### Local cross-membrane flux

At 40°C and with a typical microporous membrane,<sup>21,25,27</sup> the butanol/water vapor mixture lies in the transition region between continuum<sup>74</sup> and Knudsen transport<sup>75,76</sup> (i.e., we find a Knudsen number of approximately 8 for 0.2- $\mu\text{m}$  diameter pores<sup>77</sup>). We follow Veldsink et al.<sup>78</sup> in describing steady butanol and water fluxes through the membrane pores (in the  $x$  direction) with the classical convective-diffusion equation for a binary system<sup>74</sup>

$$N_i = C_i v - D_{BW} (dC_i/dx) \quad i = B, W \quad (1)$$

where  $C_i$  is the molar concentration of  $i$  in the vapor phase and  $D_{BW}$  is the Bosanquet-averaged<sup>79–81</sup> binary diffusion coefficient of the butanol/water vapor mixture in the membrane pores. Because gas pressure in the membrane pores is low, pore vapor is well approximated as ideal. We take  $D_{BW}$  as constant consistent with gas-phase ideality. Equation 1 accounts for both convective pressure-driven flux and diffusive flux through the membrane. Solvent transmembrane flux is zero due to the assumption that the receiving solvent is non-volatile. In general, the flow velocity,  $v$ , is not constant because the vapor is compressible. However, for thin membranes, compressibility effects are insignificant. Thus, gas convective flow obeys Darcy's law

$$v = \frac{\kappa}{\mu} \left( -\frac{\Delta P}{L_m} \right) \quad (2)$$

where  $\kappa$  is the membrane gas permeability and  $\mu$  is the vapor-mixture viscosity (both taken as constants). Consistent with gas incompressibility, gas velocity is constant with respect to cross-membrane transport. Thus, a constant gas-phase pressure gradient across the membrane (i.e., a linear gas total-pressure profile) is imposed in Eq. 2 with a higher pressure on the feed side relative to the solvent side.

Steady mass transport through the membrane pores demands that  $dN_i/dx = 0$ . Therefore, Eq. 1 is differentiated with respect to  $x$  and solved in Appendix B for the membrane vapor-concentration profiles subject to set equilibrium compositions at the feed and solvent sides of the membrane. Once the vapor-concentration profiles are established, Eq. 1 is evaluated to give the constant membrane fluxes (in the  $x$  direction)

$$\frac{N_i}{v} = \frac{(\Lambda+1)C_i(0) - C_i(L_m)}{\Lambda} \quad i=B, W \quad (3)$$

where  $\Lambda = \exp(Pe_m) - 1$  and the cross-membrane Péclet number is defined by  $Pe_m \equiv vL_m/D_{BW}$ . In the limit of small  $Pe_m$ , molecular diffusion dominates the transmembrane flux, whereas at high Péclet number convective flow carries the flux at essentially the pore-inlet concentrations. Component fluxes vary in the  $z$  direction as the compositions in the feed and solvent streams adjust to butanol and (minimal) water transfer from the feed into the solvent stream.

If we add the concentration-profile expressions for water and butanol and substitute the ideal-gas equation of state to give the total-pressure profile, we find that this profile is not strictly linear. This means that the constant-velocity assumption in Eq. 2 is inconsistent. However, when the membrane Péclet number is small (i.e.,  $Pe_m < 0.1$ ), a nearly linear pressure profile emerges. Thus, we retain the incompressible approximation in Eq. 3 and obtain an analytic solution for the cross-membrane flux.

### Phase equilibria

We now impose phase equilibria at the two sides of the membrane<sup>82,83</sup>

$$\begin{aligned} C_i(0) &= \frac{\gamma_{iF}(0)X_{iF}(0)P_{isat}(T)}{R_g T} \quad \text{and} \\ C_i(L_m) &= \frac{\gamma_{iS}(L_m)X_{iS}(L_m)P_{isat}(T)}{R_g T} \quad i=B, W \end{aligned} \quad (4)$$

where the vapor is ideal and  $R_g$  is the gas constant. Equation 4 emphasizes the importance of appropriate phase equilibria in the MVE process. For example, transport of butanol into the solvent slightly increases water solubility and, thus, produces a tiny water flux into the solvent. Such solubilization effects must be taken into account by careful description of the phase equilibria.<sup>82,83</sup> Here, we adopt the NRTL<sup>84–87</sup> and UNIQUAC<sup>88–92</sup> models introduced by Prausnitz and coworkers<sup>82–92</sup> to provide activity coefficients for the binary water/butanol system of the feed stream and the ternary water/butanol/dodecane system of the solvent stream, respectively. Binary activity coefficients were calculated using the NRTL equation with interaction and nonrandomness parameters obtained by Gmehling and Onken<sup>93</sup> from fits to experimental butanol/water vapor/liquid equilibrium data reported by Butler et al.<sup>94</sup> Ternary activity coefficients were calculated based on vapor-liquid and liquid-liquid equilibria for the constituent binary pairs as outlined by Balasubramonian et al.<sup>73</sup> and others.<sup>94–96</sup> We performed selected calculations for water/butanol/dodecane ternary liquid-liquid phase equilibria at ambient temperature to confirm the binary parameters reported by Balasubramonian et al.<sup>73</sup> Kelvin curvature effects in the phase-equilibrium calculations prove negligible.<sup>19</sup>

By Gibbs' phase rule, temperature and compositions of the feed and solvent streams set the pressure difference across the vapor phase of the membrane. Nevertheless, pressures in the feed and solvent streams remain as independent variables because the curvatures at each side of the membrane adjust to support the gas-pressure difference. Diameters of the nonwetting membrane pores are small enough to prevent liquid entry from either side, but large enough to support bulk flow. It is the ability to support capillary-pressure differences that distinguishes MVE separations from more common permselective-membrane separation processes.

Substitution of Eq. 4 into Eq. 3 gives

$$\begin{aligned} N_i &= \frac{P_{isat}(T)}{R_g T \Lambda} [(\Lambda+1)\gamma_{iF}(0)X_{iF}(0) - \gamma_{iS}(L_m)X_{iS}(L_m)]v \\ i &= B, W \end{aligned} \quad (5)$$

Darcy's law in Eq. 2 gives the vapor-convected flow velocity

$$\begin{aligned} v &= \frac{\kappa}{\mu L_m} \\ &\left( \sum_i \gamma_{iF}(0)X_{iF}(0)P_{isat}(T) - \sum_i \gamma_{iS}(L_m)X_{iS}(L_m)P_{isat}(T) \right) \\ i &= B, W \end{aligned} \quad (6)$$

Equations 5 and 6 indicate that, in general, the driving force for an MVE separation (as in MD separations) is not linearly proportional to the chemical-potential difference across the membrane. The common linear relation between cross-membrane species flux and vapor-pressure difference<sup>18–25,31,33,34</sup> is generally inadequate for MVE. Only in the limit of small  $Pe_m$  is a linear chemical-potential driving force justified. In the range of Péclet numbers characteristic of our design (0.002–0.05), calculated water fluxes deviate up to a factor of 2 from the common linear driving-force expression while butanol fluxes are less sensitive to  $Pe_m$ . With  $Pe_m = 0.1$ , water fluxes deviate by a factor of 3.

### Mass transfer

Membrane liquid inlet and outlet compositions in Eqs. 5 and 6 [i.e.,  $X_{iF}(0)$  and  $X_{iS}(L_m)$ ] are not those in the bulk of the flowing liquid phases because of mass-transfer resistances in the liquid boundary layers at both sides of the membrane. Thus, we write for the feed stream that<sup>74</sup>

$$N_i = X_{iF}(0)[N_B + N_W] + k_{XiF}[X_{iF} - X_{iF}(0)] \quad i=B, W \quad (7)$$

and for the solvent stream that

$$N_i = k_{XiS}[X_{iS}(L_m) - X_{iS}] \quad i=B, W \quad (8)$$

where  $k_{Xi}$  is the mole-fraction mass-transfer coefficient of component  $i$  in the feed or solvent flows. Equation 8 is the dilute limit of Eq. 7, because butanol and water are both dilute in the zero-membrane-flux solvent. Nonlinearities in Eqs. 5–8 prevent expression of the cross-membrane fluxes as a ratio of a driving force to a resistance.

We obtain the mass-transfer coefficients in the feed and solvent streams for water and butanol species by the length-averaged Graetz–Lévêque analysis.<sup>19,25,51,74,97,98</sup> Woven-fiber mats are used as spacers in the channel gaps<sup>19,99,100</sup> giving approximately plug flow through the channels. Open-slit (i.e., parabolic) flow gives almost identical results for the mass-transfer coefficients. Membrane-process average mass-transfer coefficients are  $k_x \sim 0.5 \text{ mol/m}^2/\text{s}$ <sup>101</sup> depending strongly on the gap thickness. As with most liquid-phase membrane processes,<sup>53,47,49,68–72,101</sup> mass-transfer resistances contribute significantly to MVE separation efficiency. Appendix C summarizes the mass-transfer analysis.

### Local mass conservation

Feed and solvent mole fractions and flows vary in the  $z$  direction; they must obey axial mass conservation to complete

**Table 1. Base Parameters for MVE Unit**

$a_L$	20 m
$D$	$1.2 \times 10^{-5} \text{ cm}^2/\text{s}^{102}$
$D_{BW}$	$2.67 \times 10^{-2} \text{ cm}^2/\text{s}^a$
$F_o$	3 mol/s
$k_X$	$0.66 \text{ mol}/\text{m}^2/\text{s}$
$L$	1.5 m
$L_m$	80 $\mu\text{m}$
$P_{Bsat} (40^\circ\text{C})$	2.50 kPa <sup>103</sup>
$P_{Wsat} (40^\circ\text{C})$	7.37 kPa <sup>104</sup>
$S_L$	0.5 mol/s
$X_{BF0}$	0.005 <sup>17</sup>
$X_{BSL}$	0
$X_{WSL}$	0
$\delta$	0.5 mm
$\eta$	$0.01 \text{ g}/\text{cm}/\text{s}^{74}$
$\kappa$	$0.03 \mu\text{m}^{2b}$
$\mu$	$10^{-4} \text{ g}/\text{cm}/\text{s}^{74}$

<sup>a</sup>Calculated from  $D_{BW} = \phi D_{BW}^{\text{gas}} / \tau$  where  $D_{BW}^{\text{gas}}$  is the effective-Bosanquet binary vapor diffusion coefficient in the porous membrane ( $= 0.06 \text{ cm}^2/\text{s}$ ) [i.e., calculated from the Bosanquet equation:  $D_{BW}^{\text{gas}} = 1 / (D_{kn}^{-1} + D_{BWmol}^{-1})$ ]<sup>79–81</sup> where  $D_{kn}$  is the Knudsen diffusion coefficient ( $= 0.2 \text{ cm}^2/\text{s}$ )<sup>75,76</sup> and  $D_{BWmol}$  is the butanol/water binary vapor diffusion coefficient ( $= 0.08 \text{ cm}^2/\text{s}$ ) scaled from Wong and Hayduk<sup>105</sup> using Chapman-Enskog theory<sup>74</sup>;  $\phi$  is membrane porosity ( $= 0.8^{21}$ ); and  $\tau$  is membrane tortuosity ( $= 1.8^{25}$ ).

<sup>b</sup>Scaled by Carman-Kozeny theory<sup>74</sup> to a pore diameter of 0.2  $\mu\text{m}$  from hydraulic permeability measurements of Cappello et al.<sup>77</sup>

the design analysis. At steady state, butanol, and water mass conservation in the feed and solvent streams over a differential length  $dz$  read

$$\frac{d(FX_{iF})}{dz} + N_i a_L = 0 \quad i = B, W \quad (9)$$

$$\frac{d(SX_{iS})}{dz} + N_i a_L = 0 \quad B, W \quad (10)$$

and

$$\frac{d(SX_{DS})}{dz} = 0 \quad (11)$$

where  $F$  and  $S$  are the local molar flow rates of the feed and solvent streams, and  $a_L$  is the cross-membrane transfer area per unit length of the MVE unit. For example, in a plate-and-frame module,  $a_L$  equals twice the channel width. Equation 11 assumes a nonvolatile solvent. As described in Appendix D, Eqs. 5–11 are solved numerically by a finite-difference scheme, given the inlet feed and solvent flows and compositions.

## Results

We consider a prototype MVE unit of feed throughput at 3 mol/s (195 L/h)<sup>18,29,32</sup> with an area per unit flow-channel length of 20 m,<sup>18,29,32</sup> and a spacer-channel gap thickness and length of 0.5 mm and 1.5 m, respectively (i.e., the total membrane area is 30 m<sup>2</sup>).<sup>18,29,32,101</sup> For a plate-and-frame module, this design corresponds, for example, to a stack of 10 membranes in parallel, each 1 m wide and 1.5 m long. Feed-to-solvent molar flow ratio is set at 6. Inlet feed is dilute butanol in water at a butanol mole fraction of 0.005 (2 wt %), close to the current tolerance limit for biofuel microbes.<sup>17</sup> The solvent enters free of butanol and water. Table 1 gives all base-design parameters.<sup>102–105</sup> With these parameters, the membrane Péclet number is less than 0.05; membrane transport is diffusion-controlled. The MVE unit

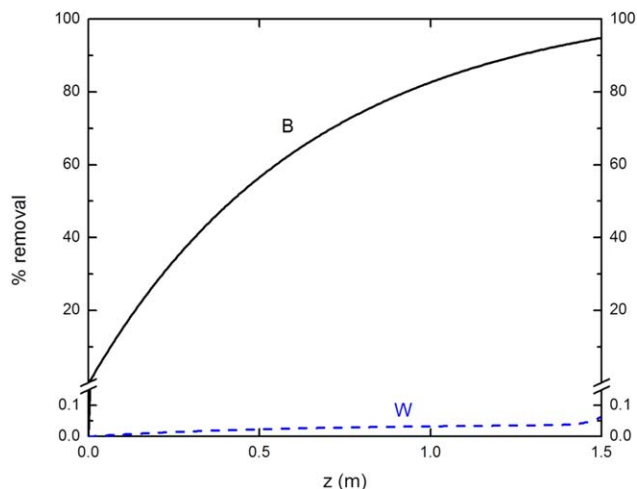


**Figure 3. Percent removal of butanol (B) and water (W) from the feed stream in the  $L = 1.5 \text{ m}$  MVE unit. 95% of butanol is removed, whereas 0.06% of water is removed.**

[Color figure can be viewed in the online issue, which is available at [wileyonlinelibrary.com](http://wileyonlinelibrary.com).]

may be of plate-and-frame, double-spiral-wound,<sup>29,32</sup> or hollow-capillary construction.

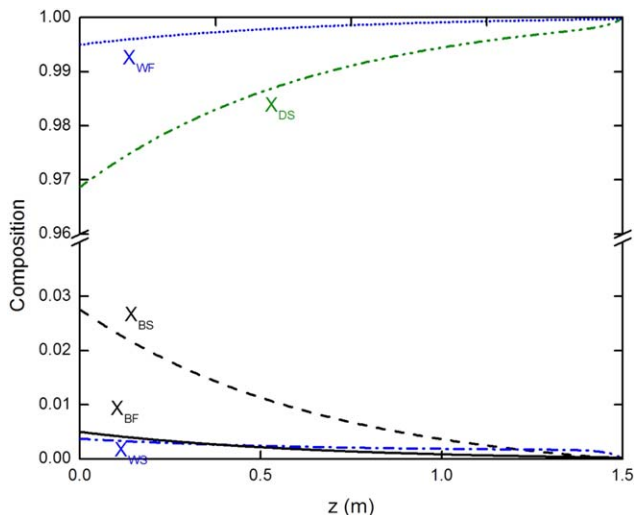
Figure 3 shows the percentage-removed axial profiles of water and butanol in the feed stream.  $z = 0$  is the feed inlet (also the extract outlet) and  $z = L$  is the solvent inlet (also the raffinate outlet). Over 90% of the feed butanol is recovered by the solvent stream within a 1.5-m long unit. Increasing solvent flow by a factor of 3 increases butanol recovery to essentially 100%. The ordinate scale change at lower-percent removals highlights water membrane transport. Water removal from the feed is less than 0.1%. As opposed to MD where the higher volatility of water compared to butanol transports considerable water across the membrane, near insolubility of water in dodecane chokes membrane water crossover. Thus, MVE behaves like pervaporation but without need for synthesizing specialized membranes to obtain high permselectivity to butanol.

Figure 4 shows axial composition profiles of the feed and solvent streams along the countercurrent MVE unit. To visualize unit-separation behavior, the ordinate is presented on two scales. Butanol mole fraction,  $X_{BF}$ , in the raffinate is nearly zero. Because the feed-to-solvent molar flow ratio is larger than unity, butanol molar concentration in the extract is enhanced here by a factor of almost 6. Likewise, because the solubility of water in dodecane is very low, essentially all water in the feed is retained. The separation or enrichment factor of butanol relative to water, defined by

$$\alpha_{BW} \equiv \frac{X_{BS0}/X_{BF0}}{X_{WS0}/X_{WF0}} \quad (12)$$

is  $\sim 1500$ . In pervaporation units, separation factors of butanol relative to water are typically around 50.<sup>17</sup> In MVE, overall recoveries of butanol from the feed stream and retention of water in the feed stream are over 90%.

Figure 5 shows membrane-flux profiles for the unit. Butanol membrane flux at the feed inlet is about  $1.2 \times 10^{-3} \text{ mol}/\text{m}^2/\text{s}$  ( $0.34 \text{ kg}/\text{m}^2/\text{h}$ ). If solvent flow increases to 3 mol/s, equal to that of the feed, butanol inlet flux increases to



**Figure 4.** Mole-fraction profiles of butanol (solid line) and water (dotted line) in feed and butanol (dashed line), water (dot-dashed line) and dodecane (double-dot-dashed line) in solvent. Butanol enters in the feed at  $X_{BF0} = 0.005$  (2 wt %) while water and butanol enter in the solvent at  $X_{WSL} = X_{BSL} = 0$ .

[Color figure can be viewed in the online issue, which is available at [wileyonlinelibrary.com](http://wileyonlinelibrary.com).]

0.59 kg/m<sup>2</sup>/h. Higher feed butanol concentrations lead to considerably high flux. Reported fluxes for recovery of 2 wt % aqueous butanol with highly selective pervaporation membranes are 0.5 kg/m<sup>2</sup>/h.<sup>17</sup>

Notwithstanding the minimal solubility of water in dodecane, Figures 3–5 demonstrate that some water transfers into the solvent because butanol uptake in the solvent enhances water solubility. In Figure 5, the enhanced flux of water at the solvent inlet ( $z = L$ ) is due to the absence of water (and butanol) in the supplied solvent. If water is present in the entering solvent, the strong increase in water flux near the solvent inlet is no longer present.

Increasing unit throughput or decreasing unit length decreases residence time and, accordingly, erodes performance. For example, with the base parameters in Table 1, a feed throughput of 5 mol/s (325 L/h) or a MVE-unit length of 0.7 m reduces butanol removal to 80%. However, separation factors and membrane fluxes are not highly sensitive to changes in flow rate or unit length because mass transfer is not membrane-transport limited (see Appendix C).

Figure 6 shows the inlet butanol membrane flux ( $z = 0$ ) as a function of mass-transfer coefficient. Not until mass-transfer coefficients greater than 10 mol/m<sup>2</sup>/s are attained does the separation unit become membrane-transport limited. As shown in Figure C1, increased liquid flows do not reduce the mass-transfer resistance except at very high flows. For  $k_x \geq 10$  mol/m<sup>2</sup>/s, the intrinsic MVE membrane flux is  $5 \times 10^{-3}$  mol/m<sup>2</sup>/s (1.4 kg/m<sup>2</sup>/h) demonstrably higher than those achieved in pervaporation separation of 2 wt % butanol from water.<sup>17</sup> However, the resulting high flows are impractical as these reduce residence time and degrade separation efficiency. As discussed in Appendix C and illustrated in Figure C1, a practical approach to decrease mass-transfer resistance is to reduce channel gap sizes. Our 0.5-mm gap size is close to a practical minimum.<sup>18</sup>

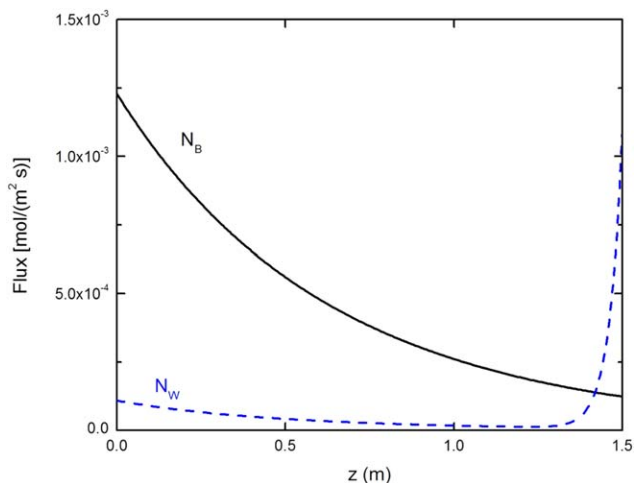


**Figure 5.** Butanol and water-flux profiles,  $N_B$  and  $N_W$ , respectively, in the 1.5-m MVE unit. Flux of butanol decreases along the axial position as the driving force diminishes.

[Color figure can be viewed in the online issue, which is available at [wileyonlinelibrary.com](http://wileyonlinelibrary.com).]

## Discussion

Our design analysis for MVE allows optimization of membrane processes to separate biosolutes from dilute aqueous solutions.<sup>10</sup> Use of MD to recover butanol from water is not effective because a significant amount water transfers across the membrane due to the higher volatility of water compared to that of butanol. Area per unit volume of the base-case MVE unit of Table 1 is 4000 m<sup>2</sup>/m<sup>3</sup> (1200 ft<sup>2</sup>/ft<sup>3</sup>), exceeding considerably those in classical liquid-liquid extraction units.<sup>101,106</sup> Further, MVE does not require phase dispersion and coalescence.

Our calculations indicate that MVE can remove and recover dilute butanol from water with fluxes somewhat higher than those in pervaporation.<sup>10,17</sup> However, MVE has a number of important advantages. For the butanol/water system, separation factors in MVE are very large, of order 1000, depending on choice of solvent. MVE has very low thermal energy requirements. Because pressures are near atmospheric, no

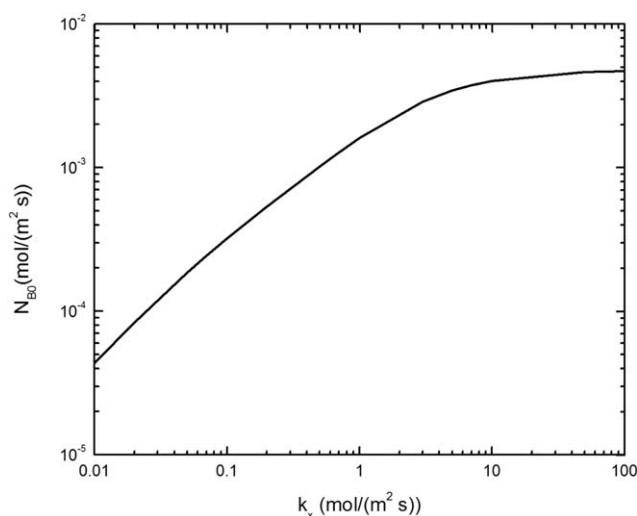


**Figure 6.** Influence of mass-transfer coefficient on inlet butanol membrane flux,  $N_{BO}$ , in the 1.5-m MVE unit. Base-case mass transfer coefficient is  $k_x = 0.66$  mol/m<sup>2</sup>/s.

vacuum need be applied. MVE equipment is compact; the process is simple and easy to operate: only liquid pumping is necessary. Most important, because MVE uses microporous membranes, it does not rely on synthesizing specialized permselective membranes for each new aqueous biosolute.

As with most membrane separations,<sup>47,49,68–72,77,101,106</sup> flow-channel mass-transfer resistances limit the membrane flux in MVE. Small gap sizes or turbulent flow are necessary to reduce these resistances. However, the large throughputs in turbulent flow reduce residence times making solute recoveries impractical. Concurrent with most membrane-separation applications, additional effort is needed to improve the mass-transfer behavior of membrane processes.<sup>47,99,100,107</sup> The important role of external mass-transfer resistance applies not only to production-scale units but also to laboratory and bench-scale apparatus.

Aside from small membrane fluxes, probably the main disadvantage of MVE (as for pervaporation and MLE) is possible fouling. The small gaps necessary to reduce mass-transfer resistance are vulnerable to plugging. Prefiltration to remove bacteria, yeast, and/or debris may be necessary. This is especially true when the channel gaps are occupied by spacers. Fouling can also erode the necessary nonwetting properties of the membrane. Establishing and maintaining complete nonwetting by both feed and solvent is a challenge, especially as membrane materials like polypropylene and Teflon<sup>®</sup> are wetted by low-tension organic solvents.<sup>34</sup> Recent advances in the development of omniphobic membranes for DCMD appear promising.<sup>34</sup> Nevertheless, periodic cleaning may be necessary. There is also a tradeoff between small pore sizes that minimize liquid pore entry and large pore sizes that minimize membrane transport resistance. Fortunately, if the largest pores inhibit liquid entry, pore-size distribution is not a crucial design feature.

We have not considered details of the downstream recovery of butanol (and water) from the product solvent, presumably by distillation. The same issue arises in pervaporation separation units that concentrate a 2 wt % butanol aqueous feed to about 20 wt % in the condensate.<sup>17</sup> With a feed-to-solvent molar flow ratio of 6, our base-parameter design achieves about a sixfold increase in butanol molar concentration from 0.5 to ~3 mol %. However, due to the high molecular weight of dodecane, the butanol mass concentration remains relatively low, at 1.2 wt %. Nevertheless, butanol is concentrated significantly relative to water in the rich solvent. The extract dodecane-free aqueous composition is 97 wt % butanol and 3 wt % water, significantly more than that achieved in pervaporation. The resulting downstream separation of butanol from water in pervaporation is more challenging than is separation of butanol from an organic solvent in MVE. With MVE, the final mixture of biosolute and dodecane can readily be separated by a rectification-only distillation column. Further, no reheating of the raffinate is required as in pervaporation.

Finally, flow-channel axial pressure drops must be small to prevent membrane liquid pore entry by either feed or solvent at their high-pressure channel entrances. Capillary-pressure differences between the liquid and vapor at the two membrane surfaces cannot exceed the pore-entry pressure. With the flows considered here, flow-channel pressure drops are much less than those anticipated to drive liquid pore entry. Thin, small pore-size, omniphobic membrane coatings may provide further protection against pressure-induced liquid invasion.

We have not optimized the MVE process, nor considered process economics. For example, solvent choice or operating conditions, such as temperature, might improve process performance.

The design analysis presented here permits such scoping calculations.

Our proposed MVE process appears feasible; it is consistent with the laws of thermodynamics (see Appendices A and E) and is more efficient than its closest competitor, pervaporation. Because extraction by MVE exhibits a very high separation factor, avoids liquid/liquid dispersion and coalescence, does not require specific permselective membranes, and consumes minimal energy, MVE provides a promising method for removal and recovery of bioproducts.

## Conclusions

A systematic design model is presented to establish viability of membrane separation processes. We focus on reducing bio-butanol concentration to nontoxic levels in a fermenter and recovering the butanol via MVE. In MVE, aqueous butanol is vaporized at the upstream face of a microporous, omniphobic, microporous membrane, and absorbed isothermally at the downstream face into a nonvolatile solvent. The solvent is highly favorable for the solute, but highly unfavorable to water. Rejection of water by the solvent makes the membrane behave effectively as permselective to solute(s) as in pervaporation. MVE is conceptually similar to MLE but with the important difference that transport through the membrane is entirely in the vapor phase.

An illustrative MVE-process-unit design is described for separation of 2 wt % butanol from water into dodecane at 40°C. In a 30 m<sup>2</sup>, 1.5-m long separator with a throughput of 200 L/h, over 90% of the butanol is recovered while water loss from the feed is nil. Thus, separation factors are over 1000 compared to about 50 in pervaporation processes. Similar to pervaporation, MVE butanol fluxes are near 0.5 kg/m<sup>2</sup>/h, limited primarily by external mass-transfer resistances. MVE units are compact, easy to operate, and consume very little energy. MVE has significant advantage over classical liquid-liquid extraction because the two liquids do not contact each other directly.

We establish the feasibility of MVE for removing and recovering dilute butanol from a 2 wt % aqueous mixture while retaining essentially all of the feed water. Proof of concept for MVE requires experimental studies. The proposed design analysis provides a framework to evaluate the performance of membrane separations.

## Acknowledgments

The authors thank William Koros and Gregory Schoofs for helpful advice. For financial support, APS thanks Brazilian Science without Borders Program under CNPq of the Brazilian Ministry of Science and Technology.

## Notation

$a_L$	= area per unit length of membrane
$Bi \equiv hL_m/k_m$	= membrane Biot number
$C_i$	= molar concentration of butanol or water in the vapor phase
$\tilde{C}_P$	= molar heat capacity
$D$	= binary diffusivity of butanol or water in the liquid feed and solvent streams
$D_{BW}$	= binary diffusivity in the membrane
$e_x$	= energy flux through membrane
$F$	= molar flow rate of feed
$g_s$	= volumetric entropy production rate
$Gz \equiv Pe(\delta/L)$	= Graetz number
$h$	= heat-transfer coefficient

$\bar{H}_i$  = partial molar enthalpy of  $i$   
 $\hat{H}_i$  = molar enthalpy of pure  $i$   
 $\Delta\bar{H}_{i\text{vap}}$  = molar enthalpy of vaporization of pure  $i$   
 $k_m$  = thermal conductivity of membrane  
 $k_X$  = mole-fraction mass-transfer coefficient for butanol or water in feed and solvent streams  
 $K$  = integration constant in Eq. A17  
 $L$  = axial length of MVE unit  
 $L_c$  = flow-channel entrance length  
 $L_m$  = thickness of membrane  
 $N_i$  = molar flux of butanol or water through membrane  
 $P$  = pressure  
 $P_{i\text{sat}}$  = vapor pressure of  $i$   
 $Pe \equiv \langle v \rangle \delta / D$  = channel Péclet number for feed or solvent flows  
 $Pe_m \equiv vL_m / D_{\text{BW}}$  = membrane Péclet number  
 $Pe_T = (\sum_i \bar{C}_{Pi} N_i L_m) / k_m$  = membrane thermal Péclet number  
 $Pr = v / \alpha$  = Prandtl number of feed or solvent streams  
 $Q = F_o / \bar{\rho}$  = feed volumetric flow rate  
 $R_g$  = ideal-gas constant  
 $S$  = molar flow rate of solvent  
 $\bar{S}_i$  = partial molar entropy of species  $i$   
 $Sc = v / D$  = Schmidt number of feed or solvent streams  
 $Sh \equiv \frac{k_X \delta}{\bar{\rho} D}$  = Sherwood number of feed or solvent streams  
 $St = a_L L h / F \bar{C}_{PF}$  = Stanton number  
 $T$  = absolute temperature  
 $v$  = superficial flow velocity of vapor phase through membrane  
 $\langle v \rangle$  = average axial channel flow velocity of MVE unit  
 $x$  = linear coordinate through membrane  
 $X_i$  = mole fraction of butanol, water, or dodecane in feed and solvent streams  
 $z$  = axial coordinate along the flow channel of MVE unit  
 $\bar{z} = z/L$ , dimensionless axial position

### Greek symbols

$\alpha$  = thermal diffusivity of feed or solvent streams  
 $\alpha_{\text{BW}}$  = separation factor defined in Eq. 12  
 $\beta$  = constant defined in Eq. A15  
 $\gamma$  = constant defined in Eq. A16  
 $\gamma_i$  = liquid-phase activity coefficient of feed or solvent streams  
 $\delta$  = flow-channel gap thickness  
 $\eta$  = viscosity of liquid feed or solvent stream  
 $\kappa$  = hydrodynamic permeability of membrane  
 $\Lambda = \exp(Pe_m) - 1$  = parameter appearing in Eq. 3  
 $\mu$  = viscosity of vapor phase in membrane pores  
 $\mu_i$  = chemical potential of species  $i$   
 $\nu$  = kinematic viscosity of feed or solvent streams  
 $\rho$  = mass density of liquid feed or solvent streams  
 $\bar{\rho}$  = molar density of liquid feed or solvent streams  
 $\tau$  = membrane tortuosity  
 $\varphi$  = membrane porosity

### Subscripts

B = butanol  
 D = dodecane  
 F = feed  
 $i$  = species  $i$   
 loc = local  
 L = outlet or liquid  
 m = membrane  
 $o$  = inlet  
 S = solvent  
 T = thermal  
 W = water

### Superscripts

E = excess  
 $^\circ$  = pure liquid  
 $\sim$  = molar  
 $\bar{\quad}$  = partial molar

### Literature Cited

- Park C-H, Geng Q. Simultaneous fermentation and separation in the ethanol and ABE fermentation. *Sep Purif Methods*. 1992;21:127–174.
- Campos EJ, Blaschek HP, Qureshi N. Production of acetone butanol ethanol from degermed corn using *Clostridium beijerinckii* BA101. *Appl Biotechnol Biochem*. 2002;99–100:553–561.
- Huang YL, Zhang L, Wu Z, Cheung CM, Yang S-T. Production of carboxylic acids from hydrolyzed corn meal by immobilized cell fermentation in a fibrous-bed bioreactor. *Bioresour Technol*. 2002; 82:51–59.
- Garg SK, Jain A. Fermentative production of 2,3-butanediol: a review. *Bioresour Technol*. 1995;51(2–3):103–109.
- van Leeuwen BNM, van der Wulp AM, Duijnste I, van Maris AJA, Straathof AJJ. Fermentative production of isobutene. *Appl Microbiol Biotechnol*. 2012;93(4):1377–1387.
- Yang J, Xian M, Su S, Zhao G, Nie Q, Jiang X, Zheng Y, Liu W. Enhancing production of bio-isoprene using hybrid MVA pathway and isoprene synthase in *E. coli*. *PLoS One*. 2012;7(4): e33509.
- Rodríguez BA, Stowers CC, Pham V, Cox BM. The production of propionic acid, propanol and propylene via sugar fermentation: an industrial perspective on the progress, technical challenges and future outlook. *Green Chem*. 2014;16:1066–1076.
- Papoutsakis ET. Engineering solventogenic clostridia. *Curr Opin Biotechnol*. 2008;19:420–429.
- Gottschal JC, Morris JG. The induction of acetone and butanol production in cultures of *Clostridium acetobutylicum* by elevated concentrations of acetate and butyrate. *FEMS Microbiol Lett*. 1981; 12:385–389.
- Groot WJ, van der Lans RGJM, Luyben KCAM. Review: technologies for butanol recovery integrated with fermentations. *Process Biochem*. 1992;27:61–75.
- Ramey DE. *Continuous Two Stage, Dual Path Anaerobic Fermentation of Butanol and Other Organic Solvents Using Two Different Strains of Bacteria*. U.S. Patent 5,753,474. 1996.
- Ramey D, Yang S-T. *Production of butyric acid and butanol from biomass*. Morgantown, WV: U.S. Department of Energy, 2004.
- Yukihiko T. High butanol production by *Clostridium saccharoperbutylacetonicum* N1-4 in fed-batch culture with pH-stat continuous butyric acid and glucose feeding method. *J Biosci Bioeng*. 2004;98:263–268.
- Qureshi N, Li X-L, Hughes S, Saha BC, Cotta MA. Butanol production from corn fiber xylan using *Clostridium acetobutylicum*. *Biotechnol Prog*. 2006;22:673–680.
- Fischer CR, Klein-Marcuschamer D, Stephanopoulos G. Selection and optimization of microbial hosts for biofuels production. *Metab Eng*. 2008;10:295–304.
- Suszkiv J. Banking on biobutanol. *Agric Res*. 2008;56(9):8–9.
- Huang HJ, Ramaswamy S, Liu Y. Review: separation and purification of biobutanol during bioconversion of biomass. *Sep Purif Technol*. 2014;132:513–540.
- Mulder M. *Basic Principles of Membrane Technology*. Dordrecht, The Netherlands: Kluwer Academic Publishers, 1996.
- Lawson KW, Lloyd DR. Review: membrane distillation. *J Membr Sci*. 1997;124:1–25.
- Curcio E, Drioli E. Membrane distillation and related operations—a review. *Sep Purif Rev*. 2005;34(1):35–86.
- Alklaibi AM, Lior N. Membrane-distillation desalination: status and potential. *Desalination*. 2005;171(2):111–131.
- El-Bourawi MS, Ding Z, Maa R, Khayet M. Review: a framework for better understanding membrane distillation separation process. *J Membr Sci*. 2006;285:4–29.
- Khayet M, Matsuura T. *Membrane Distillation: Principles and Concepts*. Oxford, UK: Elsevier, 2011.
- Khayet M. Membranes and theoretical modeling of membrane distillation: a review. *Adv Colloid Interface Sci*. 2011;164:56–88.
- Alkhdhiri A, Darwish N, Hilal N. Membrane distillation: a comprehensive review. *Desalination*. 2012;287:2–18.
- Jönsson AS, Wimmerstedt R, Harrysson AC. Membrane distillation – a theoretical study of evaporation through microporous membranes. *Desalination*. 1985;56:237–249.
- Drioli E, Calabrò V, Wu Y. Microporous membranes in membrane distillation. *Pure Appl Chem*. 1986;58(12):1657–1662.
- Lawson KW, Lloyd DR. Membrane distillation. II. Direct contact MD. *J Membr Sci*. 1996;120:123–133.

29. Koschikowski J, Wieghaus M, Rommel M. Solar thermal-driven desalination plants based on membrane distillation. *Desalination*. 2003;156:295–304.
30. El-Bourawi MS, Ding Z, Maa R, Khayet M. A framework for better understanding membrane distillation separation process. *J Membr Sci*. 2006;285:4–29.
31. Chen TC, Ho CD, Yeh HM. Theoretical modeling and experimental analysis of direct contact membrane distillation. *J Membr Sci*. 2009;330:279–287.
32. Winter D, Koschikowski J, Wieghaus M. Desalination using membrane distillation: experimental studies on full scale spiral wound modules. *J Membr Sci*. 2011;375:104–112.
33. Godino LP, Peña L, Mengual JI. Membrane distillation: theory and experiments. *J Membr Sci*. 1996;121:83–93.
34. Lin S, Nejati S, Boo C, Hu Y, Osuji CO, Elimelech M. Omniphobic membrane for robust membrane distillation. *Environ Sci Technol Lett*. 2014;1:443–447.
35. Lin S, Yip NY, Elimelech M. Direct contact membrane distillation with heat recovery: thermodynamic insights from module scale modeling. *J Membr Sci*. 2014;453:498–515.
36. Francis L, Ghaffour N, Alsaadi AS, Nunes SP, Amy GL. Performance evaluation of the DCMD desalination process under bench scale and large scale module operating conditions. *J Membr Sci*. 2014;455:103–112.
37. Ghadiri M, Fakhri S, Shirazian S. Modeling of water transport through nanopores of membranes in direct-contact membrane distillation process. *Polym Eng Sci*. 2014;55(3):660–666.
38. Kim AS. Cylindrical cell model for direct contact membrane distillation (DCMD) of densely packed hollow fibers. *J Membr Sci*. 2014;455:168–186.
39. Manawi YM, Khraisheh M, Fard AK, Benyahia F, Adham S. Effect of operational parameter on distillate flux in direct contact membrane distillation (DCMD): comparison between experimental and model predicted performance. *Desalination*. 2014;336:110–120.
40. Sarti GC, Gostoli C, Bandini S. Extraction of organic-compounds from aqueous streams by vacuum membrane distillation. *J Membr Sci*. 1993;80:21–33.
41. Banat FA, Simandl J. Removal of benzene traces from contaminated water by vacuum membrane distillation. *Chem Eng Sci*. 1996;51(8):1257–1265.
42. Lawson KW, Lloyd DR. Membrane distillation. I. Module design and performance evaluation using vacuum membrane distillation. *J Membr Sci*. 1996;120:111–121.
43. Sun AC, Kosar W, Zhang Y, Feng X. Vacuum membrane distillation for desalination of water using hollow fiber membranes. *J Membr Sci*. 2014;455:131–142.
44. Shao F, Hao C, Ni L, Zhang Y, Du R, Meng J, Liu Z, Xiao C. Experimental and theoretical research on N-methyl-2-pyrrolidone concentration by vacuum membrane distillation using polypropylene hollow fiber membrane. *J Membr Sci*. 2014;452:157–164.
45. Khayet M, Godino P, Mengual JI. Theory and experiments on sweeping gas membrane distillation. *J Membr Sci*. 2000;165:261–272.
46. Khayet M, Godino MP, Mengual JI. Theoretical and experimental studies on desalination using the sweeping gas membrane distillation method. *Desalination*. 2003;157:297–305.
47. Zhu C, Liu GL, Cheung CS, Leung CW, Zhu ZC. Ultrasonic stimulation on enhancement of air gap membrane distillation. *J Membr Sci*. 1999;161:85–93.
48. Alsaadi AS, Ghaffour N, Li JD, Gray S, Francis L, Maab H, Amy GL. Modeling of air-gap membrane distillation process: a theoretical and experimental study. *J Membr Sci*. 2013;445:53–65.
49. Tian R, Gao H, Yang XH, Yan SY, Li S. A new enhancement technique on air gap membrane distillation. *Desalination*. 2014;332(1):52–59.
50. Francis L, Ghaffour N, Alsaadi AA, Amy GL. Material gap membrane distillation: a new design for water vapor flux enhancement. *J Membr Sci*. 2013;448:240–247.
51. Kimura S, Nakao SI, Shimatani SI. Transport phenomena in membrane distillation. *J Membr Sci*. 1987;33:285–298.
52. Sakai K, Koyano T, Muroi T. Effect of temperature polarization on water vapor permeability for blood in membrane distillation. *Chem Eng J*. 1988;38(3):B33–B39.
53. Gryta M, Karakulski MK. The application of membrane distillation for the concentration of oil–water emulsions. *Desalination*. 1991;121:23–29.
54. Qureshi N, Meagher MM, Hutkins RW. Recovery of 2,3-butanediol by vacuum membrane distillation. *Sep Sci Technol*. 1994;29(13):1733–1748.
55. Calabrò V, Jiao BL, Drioli E. Theoretical and experimental study on membrane distillation in the concentration of orange juice. *Ind Eng Chem Res*. 1994;33(71):1803–1808.
56. Tomaszewska M, Gryta M, Morawski AW. Study on the concentration of acids by membrane distillation. *J Membr Sci*. 1995;102:113–122.
57. Sudoh M, Takuwa K, Iizuka H, Nagamatsuya K. Effects of thermal and concentration boundary layers on vapor permeation in membrane distillation of aqueous lithium bromide solution. *J Membr Sci*. 1997;131:1–7.
58. Tomaszewska M, Gryta M, Morawski AW. The influence of salt in solutions on hydrochloric acid recovery by membrane distillation. *Sep Purif Technol*. 1998;14(1–3):183–188.
59. Capuano A, Menoli B, Andreucci VE, Criscuoli A, Drioli E. Membrane distillation of human plasma ultrafiltrate and its theoretical applications to haemodialysis techniques. *Int J Artif Organs*. 2000;23(7):415–422.
60. Tomaszewska M, Gryta M, Morawski AW. Mass transfer of HCl and H<sub>2</sub>O across the hydrophobic membrane during membrane distillation. *J Membr Sci*. 2000;166(2):149–157.
61. Tomaszewska M. Membrane distillation - examples of applications in technology and environmental protection. *J Environ Stud*. 2000;9(1):27–36.
62. Banat FA, Simandl J. Membrane distillation for propane removal from aqueous streams. *J Chem Technol Biotechnol*. 2000;75(2):168–178.
63. Gryta M. Concentration of aqueous solutions of caprolactam by membrane distillation. *Polimery*. 2006;51(9):665–670.
64. Tomaszewska M, Mientka A. Separation of HCl from HCl–H<sub>2</sub>SO<sub>4</sub> solutions by membrane distillation. *Desalination*. 2009;240(1–3):244–250.
65. Kesime UK, Milne N, Chu CY, Aral H, Duke M. Recovery of water and acid from leach solutions using direct contact membrane distillation. *Water Sci Technol*. 2014;69(4):868–875.
66. Hwang YL, Keller GE II, Olson JD. Steam stripping for removal of organic pollutants from water. 1. Stripping effectiveness and stripper design. *Ind Eng Chem Res*. 1992;31(7):1753–1759.
67. Hwang YL, Keller GE II, Olson JD. Steam stripping for removal of organic pollutants from water. 2. Vapor-liquid equilibrium data. *Ind Eng Chem Res*. 1992;31(7):1759–1768.
68. Kiani A, Bhavre RR, Sirkar KK. Solvent extraction with immobilized interfaces in a microporous hydrophobic membrane. *J Membr Sci*. 1984;20:125–145.
69. Kim BM. Membrane-based solvent extraction for selective removal and recovery of metals. *J Membr Sci*. 1984;21:5–19.
70. Prasad R, Sirkar KK. Dispersion-free solvent extraction with microporous hollow-fiber modules. *AIChE J*. 1988;34(2):177–188.
71. Prasad R, Sirkar KK. Membrane-based solvent extraction. In: Ho W, Sirkar KK, editors. *Membrane Handbook, Chapter 41*. New York, NY: van Nostrand Reinhold, 1992.
72. Kitiyanan B, O'Haver JH, Harwell JH, Sabatini DA. The use of liquid-liquid extraction in hollow fiber membrane for the removal of organic contaminants from aqueous surfactant systems. In: Scaemhorn JF, Harwell JH, editors. *Surfactant-Based Separations*. ACS Symposium Series, Vol. 740, Chapter 6. Washington, DC: American Chemical Society, 1999.
73. Balasubramonian S, Kumar S, Sivakumar D, Mudali UK. Application of COSMO-RS method for the prediction of liquid-liquid equilibrium of water/*n*-dodecane/1-butanol. *ISRN Thermodyn*. 2014;2014:1–6.
74. Bird RB, Stewart WE, Lightfoot EN. *Transport Phenomena, 2nd ed.*, Chapters 14, 19, 24. New York, NY: Wiley, 2006.
75. Knudsen VM. Die gesetze der molekularströmung und der inneren reibungsströmung der gase durch röhren. *Ann Phys*. 1909;29(1):75–130.
76. Satterfield CN. *Mass Transfer in Heterogeneous Catalysis*. Cambridge, MA: MIT Press, 1970:9–12, 41–42.
77. Cappello N, Pence D, Liburdy J. Mass transport limitations through porous hydrophobic membranes. In: *Proceedings of the ASME 2013 Fluids Engineering Division Summer Meeting*. Paper No. FEDSM2013-16559. Incline Village, NV: American Society of Mechanical Engineers, 2013.
78. Veldsink JW, van Damme RMJ, Versteeg GF, van Swaaij WPM. The use of the dusty-gas model for the description of mass transport in chemical reaction in porous media. *Chem Eng J*. 1995;57(2):115–125.

79. Bosanquet CH. The optimum pressure for a diffusion separation plant. British TA Report. BR/507. 1944.
80. Pollard WG, Present RD. On gaseous self-diffusion in long capillary tubes. *Phys Rev*. 1948;73:762–774.
81. Zalc JM, Reyes SC, Iglesia E. The effects of diffusion mechanism and void structure on transport rates and tortuosity factors in complex porous structures. *Chem Eng Sci*. 2004;59:2947–2960.
82. Prausnitz JM, Grens E, Anderson T, Eckert C, Hsieh R, O'Connell J. *Computer Calculations for Multicomponent Vapor-Liquid and Liquid-Liquid Equilibria*. Englewood Cliffs, NJ: Prentice-Hall, 1980.
83. Prausnitz JM, Lichtenthaler RN, de Azevedo EG. *Molecular Thermodynamics of Fluid Phase Equilibria, 3rd ed.* New Jersey: Prentice Hall, 1999.
84. Renon H, Prausnitz JM. Local compositions in thermodynamic excess functions for liquid mixtures. *AIChE J*. 1968;14:135–144.
85. Renon H, Prausnitz JM. Estimation of parameters for the NRTL equation for excess Gibbs energies of strongly nonideal liquid mixtures. *Ind Eng Chem Process Des Dev*. 1969;8:413–419.
86. Prausnitz JM, Tavares FW. Thermodynamics of fluid-phase equilibria for standard chemical engineering operations. *AIChE J*. 2004;50(4):739–761.
87. Lee BH, Qin Y, Prausnitz JM. Thermodynamic representation of ternary liquid-liquid equilibria near-to and far-from the plait point. *Fluid Phase Equilib*. 2006;240(1):67–72.
88. Abrams DS, Prausnitz JM. Statistical thermodynamics of liquid mixtures: a new expression for the excess Gibbs energy of partly or completely miscible systems. *AIChE J*. 1975;21:116–128.
89. Fredenslund A, Jones RL, Prausnitz JM. Group-contribution estimation of activity coefficients in nonideal liquid mixtures. *AIChE J*. 1975;21:1086–1099.
90. Anderson T, Prausnitz JM. Application of the UNIQUAC equation to calculation of multicomponent phase equilibria. 1. Vapor-liquid equilibria. *Ind Eng Chem Proc Des Dev*. 1978;17:552–561.
91. Anderson T, Prausnitz JM. Application of the UNIQUAC equation to calculation of multicomponent phase equilibria. 2. Liquid-liquid equilibria. *Ind Eng Chem Proc Des Dev*. 1978;17:561–567.
92. Maurer G, Prausnitz JM. On the derivation and extension of the UNIQUAC equation. *Fluid Phase Equilib*. 1978;2:91–99.
93. Gmehling J, Onken U. *Vapor-Liquid Equilibrium Data Collection: Aqueous-Organic Systems, Vol. 1, Part 1*. In: Behrens D, Eckermann R, editors. Chemistry Data Series. Frankfurt, Germany: Dechema, 1977.
94. Butler JAV, Thomson DW, MacLennan WH. The free energy of the normal aliphatic alcohols in aqueous solution. *J Chem Soc*. 1933: 674–686.
95. Nagata I, Katoh K. Effective UNIQUAC equation in phase equilibrium calculation. *Fluid Phase Equilib*. 1981;5(3–4):225–244.
96. Nagata I. Prediction of ternary phase equilibria from binary data. *Thermochim Acta*. 1982;56(1):43–57.
97. Lévêque MM. Les lois de transmission de chaleur par convection. *Ann Mines Mem*. 1928;ser 12, 13:201–299, 305–362, 381–415.
98. Newman JS, Thomas-Alyea KE. *Electrochemical Systems, 3rd ed.*, Chapter 17. Hoboken, NJ: Wiley-Interscience, 2004.
99. Sonin AA, Isaacson MS. Optimization of flow design in forced flow electrochemical systems with special application to electro dialysis. *Ind Eng Chem Proc Des Dev*. 1974;13(3):241–248.
100. Schock G, Miquel A. Mass transfer and pressure loss in spiral wound modules. *Desalination*. 1987;64:339–352.
101. Yang M-C, Cussler EL. Designing hollow-fiber contactors. *AIChE J*. 1986;32(11):1910–1916.
102. Li SFY, Onh HM. Infinite dilution diffusion coefficients of several alcohols in water. *J Chem Eng Data*. 1990;35:136–137.
103. Kemme HR, Kreps SI. Vapor pressure of primary *n*-alkyl chlorides and alcohols. *J Chem Eng Data*. 1969;14(1):98–102.
104. Gubkiv AN, Fermor NA, Smirnov NI. Vapor pressure of monopoly systems. *Zh Prikl Khim (Leningrad)*. 1964;37:2204–2210.
105. Wong C-F, Hayduk W. Molecular diffusivities for propene in 1-butanol, chlorobenzene, ethylene glycol, and *n*-octane at elevated pressures. *J Chem Eng Data*. 1990;35:323–328.
106. Mackowiak J. *Fluid Dynamics of Packed Columns – Principles of the Fluid Dynamic Design of Columns for Gas/Liquid and Liquid/Liquid Systems, 1st ed.*, Chapter 7. Berlin: Springer-Verlag, 2010.
107. Vane LM, Alvarez FR. Full-scale vibrating pervaporation membrane unit: VOC removal from water and surfactant solutions. *J Membr Sci*. 2002;202:177–193.
108. Majer V, Svoboda V. *Enthalpies of Vaporization of Organic Compounds: A Critical Review and Data Compilation*. Oxford: Blackwell Scientific, 1985:300.
109. Sinnott RK. *Coulson and Richardson's Chemical Engineering Volume 6 - Chemical Engineering Design, 4th ed.* Oxford: Elsevier, 2005:938.
110. Belousov VP, Ponner V. Heats of mixing for liquids. VI. Heats of mixing in butyl alcohol-water, isobutyl alcohol-water, and sec-butyl alcohol-water binary systems. *Vestn Leningr Univ Fiz Khim*. 1970; 10:111–115.
111. Nguyen TH, Ratcliff GA. Heats of mixing of *n*-alcohol-*n*-alkane systems at 15°C and 55°C. *J Chem Eng Data*. 1975;20:252–255.
112. French HT, Richards A, Stokes RH. Thermodynamics of the partially miscible system ethanol + hexadecane. *J Chem Thermodyn*. 1979;11(7):671–686.
113. Welty JR, Wicks CE, Wilson RE, Rorrer G. *Fundamentals of Momentum, Heat, and Mass Transfer, 4th ed.* New York: Wiley, 2001.
114. Benson GC, D'Arcy PJ. Heat capacities of binary mixtures of *n*-dodecane with hexane isomers. *Thermochim Acta*. 1986;102L:75–81.
115. Newman J. Numerical solution of coupled, ordinary differential equations. *Ind Eng Chem Fundam*. 1968;7(3):514–517.

## Appendix A : Isothermal-Module Approximation

As feed enters the MVE unit, it vaporizes at the upstream face of an omniphobic, microporous membrane. Vaporization cools the feed. Generated vapor transports enthalpy through the membrane and dissolves into the countercurrent-flowing solvent. Heat released upon vapor absorption along with mass-transported energy increase the solvent temperature. Thus, raffinate exits the MVE module cooled while extract exits warmed. The overall heating process protects membrane vapor from condensation in the pores, provided that the solvent enters at or slightly above the inlet temperature of the feed. In this appendix, we estimate that the feed and solvent temperature excursions are minimal, about a few tenths of degree Celsius. The MVE process operates essentially isothermal.

To justify the isothermal approximation, both the temperature change across the membrane (between  $x = 0$  and  $x = L_m$ ) and the axial temperature changes along the feed and solvent flow paths (between  $z = 0$  and  $z = L$ ) must be negligible. Figure A1 illustrates a typical temperature profile across the membrane at the module inlet using membrane molar fluxes calculated from the base case presented in the main text. Feed vaporizes at the upstream membrane side ( $x = 0$ ) and dissolves into solvent at the downstream membrane side ( $x = L_m$ ). Feed temperature is less than that of the solvent. Temperature increases across the membrane. Thus, thermal energy transports in the negative  $x$  direction. However, the cross-membrane fluxes carry enthalpy in the positive  $x$  direction. As the positive mass-transfer-driven enthalpy fluxes are larger than the negative thermal-driven enthalpy fluxes, net energy transfers from the colder feed stream to the hotter solvent stream. The transmembrane temperature increase seen in Figure A1 originates from latent enthalpies of phase change and from nonideal enthalpies of mixing. Because of enthalpy convected by the transmembrane vapor fluxes,  $N_i$ , net energy transfers through the membrane from the feed to the solvent stream against a slight temperature rise. The fact that energy transfers from a lower temperature in the feed to a higher temperature in the solvent may appear counterintuitive. This issue is addressed carefully in Appendix E.

To establish the feed and solvent  $z$ -temperature profiles,  $T_F(z)$  and  $T_S(z)$ , we perform axial energy balances coupled with the transmembrane temperature profiles. For the feed stream, we write

$$F\tilde{C}_{PF} \frac{dT_F}{dz} + a_L e_x(0) = 0 \quad (\text{A1})$$

where  $e_x(0) \equiv h_F(T_F - T_F(0)) + \sum_i N_i \bar{H}_{iF}(0)$  is the net transmembrane heat and mass-transfer enthalpy flux.<sup>74</sup> Likewise, for the solvent stream, we demand that

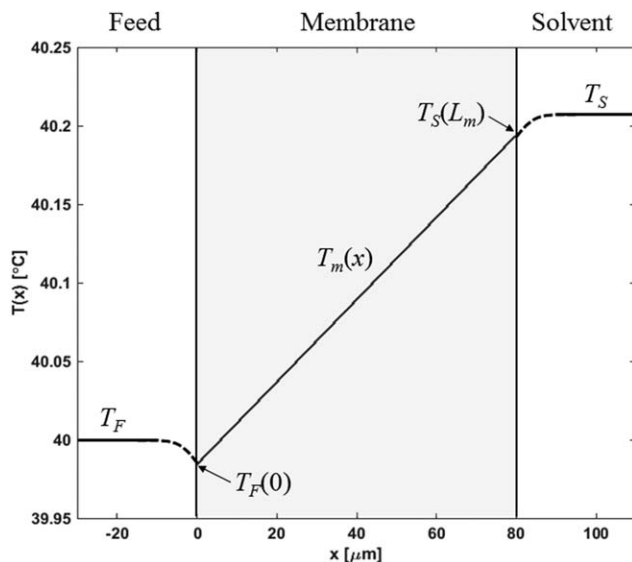


**Figure A1. Computed temperature profile across the MVE membrane at the feed inlet ( $z=0$ ) for base-case conditions. Solid lines are computed values and dashed lines are schematic for a thermal boundary layer thickness of  $10\ \mu\text{m}$ . Note that  $T_F - T_F(0) = 0.016^\circ\text{C}$ ,  $T_S - T_S(L_m) = 0.013^\circ\text{C}$ , and  $T_S(L_m) - T_F(0) = 0.210^\circ\text{C}$ . The membrane temperature profile indicates that thermal heat flux travels from the solvent to the feed membrane face. Nevertheless, because the total energy flux is directed in the positive  $x$  direction, the feed cools and the solvent warms.**

$$S\tilde{C}_{PS}\frac{dT_S}{dz} + a_L e_x(L_m) = 0 \quad (\text{A2})$$

where  $e_x(L_m) \equiv h_S(T_S(L_m) - T_S) + \sum_i N_i \tilde{H}_{iS}(L_m)$ . In these expressions,  $\tilde{C}_{PF}$  or  $\tilde{C}_{PS}$  and  $h_F$  or  $h_S$  are ideal-mixed molar heat capacities and heat-transfer coefficients for the feed or solvent streams, respectively.  $T_F(0)$  or  $T_S(L_m)$  and  $\tilde{H}_{iF}(0)$  or  $\tilde{H}_{iS}(L_m)$  are the temperatures and partial molar enthalpies of the liquid species  $i$  at positions  $x=0$  or  $x=L_m$  of the membrane faces, respectively. Our mass-balance calculations for the dilute butanol base-case indicate minimal changes in the feed and solvent flows. Thus,  $F$  and  $S$  are constant in Eqs. A1 and A2, as are heat capacities and heat-transfer coefficients.

To proceed, an expression for the local temperature difference is needed between the bulk streams and the membrane interfaces:  $T_F - T_F(0)$  and  $T_S(L_m) - T_S$ . Total energy flux through the membrane includes both that conducted and that convected. For an ideal gas in the pores of the membrane, the total energy flux  $e_x$  at each  $z$  location reads<sup>74</sup>

$$e_x = -k_m \frac{dT_m}{dx} + \sum_i \tilde{H}_i N_i \quad i=B, W \quad (\text{A3})$$

where  $k_m$  is the effective membrane thermal conductivity corresponding to butanol/water vapor mixture in the pores and to the solid matrix,  $T_m$  is the local temperature in the membrane, and  $\tilde{H}_i$  is the pure species  $i$  molar enthalpy in the ideal vapor phase. Species membrane fluxes,  $N_i$ , are constant in the  $x$  direction. The product of species flux and enthalpy carries energy across the membrane from the feed to the solvent sides in opposition to a tem-

perature increase (see Figure A1). At steady state, the divergence of the total energy flux in the  $x$  direction is zero or  $de_x/dx=0$ . Application of this constraint to Eq. A3 yields the following differential equation for the membrane temperature profiles

$$\frac{d^2 T_m}{dx^2} - \frac{\sum_i \tilde{C}_{Pi} N_i}{k_m} \frac{dT_m}{dx} = 0 \quad i=B, W \quad (\text{A4})$$

where  $\tilde{C}_{Pi}$  is the vapor molar heat capacity of pure vapor species  $i$ . Solution of Eq. A4 subject to boundary conditions  $T_m(x=0) = T_F(0)$  and  $T_m(x=L_m) = T_S(L_m)$  gives the transmembrane temperature profile at each  $z$  location

$$\frac{T_m(x) - T_F(0)}{T_S(L_m) - T_F(0)} = \frac{\exp\left(\frac{\sum_i \tilde{C}_{Pi} N_i x}{k_m}\right) - 1}{\exp\left(\frac{\sum_i \tilde{C}_{Pi} N_i L_m}{k_m}\right) - 1} \quad (\text{A5})$$

The thermal Péclet number in the membrane,  $Pe_T = (\sum_i \tilde{C}_{Pi} N_i L_m)/k_m$ , is of order  $10^{-3}$ . Consequently, Eq. A5 simplifies to a linear temperature profile

$$T_m(x) = T_F(0) + \frac{T_S(L_m) - T_F(0)}{L_m} x \quad (\text{A6})$$

Equation A6 gives the membrane temperature profile graphed in Figure A1.

To determine the membrane interface temperatures  $T_F(0)$  and  $T_S(L_m)$ , additional relations are required. For each  $z$  location at the feed/membrane interface ( $x=0$ ), continuity of the total energy flux demands that  $e_x(0) = e_x$  or

$$h_F [T_F - T_F(0)] + \sum_i \tilde{H}_{iF}(0) N_i = -k_m \left. \frac{dT_m}{dx} \right|_{x=0} + \sum_i \tilde{H}_i(0) N_i \quad (\text{A7})$$

Upon introduction of the molar enthalpy of vaporization,  $\Delta\tilde{H}_{i\text{vap}}(0)$ , of pure species  $i$  at temperature  $T_F(0)$ , and the partial-molar excess enthalpy of species  $i$  in the aqueous feed stream,  $\tilde{H}_{iF}^E(0)$ ,<sup>83</sup> Eq. A7 reduces to

$$h_F [T_F - T_F(0)] = -k_m \frac{[T_S(L_m) - T_F(0)]}{L_m} + \sum_i N_i \left( \Delta\tilde{H}_{i\text{vap}}(0) - \tilde{H}_{iF}^E(0) \right) \quad (\text{A8})$$

Similarly, continuity of the total energy flux at the solvent/membrane interface ( $x=L_m$ ) yields

$$h_S [T_S(L_m) - T_S] = -k_m \frac{[T_S(L_m) - T_F(0)]}{L_m} + \sum_i N_i \left( \Delta\tilde{H}_{i\text{vap}}(L_m) - \tilde{H}_{iS}^E(L_m) \right) \quad (\text{A9})$$

where  $h_S$  is the solvent-side heat-transfer coefficient,  $\Delta\tilde{H}_{i\text{vap}}(L_m)$  is the molar heat of vaporization of pure species  $i$  at temperature  $T_S(L_m)$ , and  $\tilde{H}_{iS}^E(L_m)$  is partial-molar excess enthalpy of species  $i$  in the solvent stream at the membrane/solvent interface.<sup>83</sup> As with mass-transfer coefficients in the main text, we assume that  $h_F = h_S = h$ . For small temperature differences across the membrane (see Figure A1), molar enthalpies of vaporization are temperature independent, as are liquid partial-molar enthalpies. Subtraction of Eq. A9 from Eq. A8 indicates that the temperature decline between the bulk feed and the membrane differs from the temperature difference between the membrane and the bulk solvent because of nonzero partial-molar excess enthalpies

$$T_F - T_F(0) = T_S(L_m) - T_S + \frac{1}{h} \sum_i \Delta \bar{H}_i^E N_i \quad (\text{A10})$$

where  $\Delta \bar{H}_i^E = \bar{H}_{iS}^E(L_m) - \bar{H}_{iF}^E(0)$  is the difference in liquid partial-molar excess enthalpies between the solvent and feed streams. Substitution of this result into Eq. A8 to eliminate  $T_S(L_m)$  reveals that

$$\begin{aligned} & T_F - T_F(0) \\ &= \left\{ Bi^{-1}(T_F - T_S) + \frac{1}{h} \sum_i \left[ \Delta \bar{H}_{i\text{vap}} - \bar{H}_{iF}^E(0) + Bi^{-1} \Delta \bar{H}_i^E \right] N_i \right\} \\ & / (1 + 2Bi^{-1}) \end{aligned} \quad (\text{A11})$$

where  $Bi \equiv hL_m/k_m$  is the membrane Biot number.

Upon choosing the pure-liquid molar enthalpies of species  $i$  at  $T_F(0)$  as reference, substitution of Eq. A11 into Eq. A1, and Eqs. A10 and A11 into Eq. A2 gives, respectively

$$\begin{aligned} & \frac{dT_F}{dz} + \frac{a_L h}{\tilde{C}_{PF}(1 + 2Bi^{-1})} \\ & \left\{ Bi^{-1}(T_F - T_S) + \frac{1}{h} \sum_i N_i \left[ \Delta \bar{H}_{i\text{vap}} + Bi^{-1} [\bar{H}_{iS}^E(L_m) + \bar{H}_{iF}^E(0)] \right] \right\} \\ & = 0 \end{aligned} \quad (\text{A12})$$

and

$$\begin{aligned} & \frac{dT_S}{dz} + \frac{a_L h}{\tilde{C}_{PS}(1 + 2Bi^{-1})} \\ & \left\{ Bi^{-1}(T_F - T_S) + \frac{1}{h} \sum_i N_i \left[ \Delta \bar{H}_{i\text{vap}} + Bi^{-1} [\bar{H}_{iS}^E(L_m) + \bar{H}_{iF}^E(0)] \right] \right\} \\ & = 0 \end{aligned} \quad (\text{A13})$$

In our estimate of the  $z$ -temperature profiles in MVE, we set the transmembrane fluxes constant (see Figure 5 for actual variations). This approximation decouples the mass and energy balances and greatly simplifies the analysis without compromising the conclusions. Likewise, partial-molar excess enthalpies in the second term on the left of Eqs. A12 and A13 are taken as temperature and composition independent.

Subtraction of Eq. A12 from Eq. A13 results in a linear ordinary differential equation for the temperature difference between the solvent and feed streams:  $\Delta T(z) \equiv T_S(z) - T_F(z)$ , or

$$\frac{d\Delta T}{d\tilde{z}} - \beta \Delta T = -\gamma \quad (\text{A14})$$

where  $\tilde{z} = z/L$  is the dimensionless axial position. Constants  $\beta$  and  $\gamma$  are defined as

$$\beta = \frac{StBi^{-1}}{1 + 2Bi^{-1}} \left( \frac{F\tilde{C}_{PF}}{S\tilde{C}_{PS}} - 1 \right) \quad (\text{A15})$$

and

$$\gamma = \frac{\frac{St}{h} \sum_i N_i \left[ \Delta \bar{H}_{i\text{vap}} + Bi^{-1} [\bar{H}_{iS}^E(L_m) + \bar{H}_{iF}^E(0)] \right]}{1 + 2Bi^{-1}} \left( \frac{F\tilde{C}_{PF}}{S\tilde{C}_{PS}} - 1 \right) \quad (\text{A16})$$

where  $St = a_L L h / F \tilde{C}_{PF}$  is a Stanton number for the feed stream. Integration of Eq. A14 gives

$$\Delta T(z) = T_S - T_F = K \exp(\beta \tilde{z}) + \gamma / \beta \quad (\text{A17})$$

where  $K$  is an integration constant. At  $\tilde{z} = 0$ ,  $T_F = T_{F0}$  and  $T_S = T_{S0}$  while at  $\tilde{z} = 1$ ,  $T_F = T_{FL}$  and  $T_S = T_{SL}$ . Feed and solvent inlet temperatures are known (in the base case, each 40°C), but  $T_{S0}$  and  $T_{FL}$  are not. Application of the stated boundary conditions in conjunction with an overall energy balance on the module (i.e.,  $(T_{S0} - T_{SL}) / (T_{F0} - T_{FL}) = F\tilde{C}_{PF} / S\tilde{C}_{PS}$ ) yields the axial temperature difference as a function of axial position

$$\begin{aligned} \Delta T(z) & \equiv T_S(z) - T_F(z) = \\ & \frac{\gamma}{\beta} \left[ 1 - \left( \frac{F\tilde{C}_{PF}}{S\tilde{C}_{PS}} - 1 \right) \frac{\exp(\beta \tilde{z})}{(F\tilde{C}_{PF} / S\tilde{C}_{PS}) \exp(\beta) - 1} \right] \end{aligned} \quad (\text{A18})$$

Equation A18 estimates the profile of temperature difference between the feed and solvent flows. However, we also seek expressions for the temperature profiles of the feed and solvent streams,  $T_F$  and  $T_S$ , independently. To obtain these temperature profiles, we relate temperatures  $T_F$  and  $T_S$  by an energy balance over a control volume from  $z = 0$  to an arbitrary axial position  $z$

$$T_S(z) = \frac{F\tilde{C}_{PF}}{S\tilde{C}_{PS}} [T_F(z) - T_{F0}] + T_{S0} \quad (\text{A19})$$

Combination of Eqs. A18 and A19, and the overall module energy balance above gives the feed temperatures as a function of axial position

$$T_F(z) = T_{F0} + \frac{\Delta T(z) - \frac{F\tilde{C}_{PF}}{S\tilde{C}_{PS}} \Delta T(L)}{\left( \frac{F\tilde{C}_{PF}}{S\tilde{C}_{PS}} - 1 \right)} \quad (\text{A20})$$

where  $\Delta T(z)$  and  $\Delta T(L)$  obey Eq. A18 evaluated at  $z$  and  $z = L$ , respectively. Finally, the solvent temperature profile follows by definition and from Eq. A20

$$T_S(z) = \Delta T(z) + T_F(z) \quad (\text{A21})$$

Evaluation of the temperature profiles from Eqs. A19, A20, and A21 requires values for  $N_i$  and  $\Delta \bar{H}_{i\text{vap}}$  of butanol and water,  $\tilde{C}_{PF}$ ,  $\tilde{C}_{PS}$ ,  $h$ , and  $k_m$  in addition to the base-case values listed in Table 1. Based on Figure 5, we take  $N_i$  for both water and butanol to be the maximum predicted flux at any axial position along the membrane, which is  $10^{-3}$  mol/m<sup>2</sup>/s. Thus, we calculate the largest possible temperature difference. Molar enthalpies of vaporization for butanol and water are 52 and 41 kJ/mol,<sup>108,109</sup> respectively. Partial-molar excess enthalpies for butanol and water in the binary feed and ternary solvent mixtures are estimated from tabulated heats of mixing for binary mixtures.  $\bar{H}_{BF}^E(0)$  and  $\bar{H}_{WF}^E(0)$  for butanol/water mixtures are estimated as  $-7$  and  $0$  kJ/mol, respectively at 30°C.<sup>110</sup> In the absence of data on the ternary butanol/water/dodecane system, we estimate  $\bar{H}_{BS}^E(L_m)$  as 5 kJ/mol from the binary butanol/dodecane mixture at 55°C.<sup>111</sup> Likewise, we estimate  $\bar{H}_{WS}^E(L_m)$  as 10 kJ/mol from the binary ethanol/hexadecane mixture at 35°C.<sup>112</sup> Calculated temperature profiles are insensitive to the estimates for excess enthalpies. Molar heat capacities of the feed and solvent are taken as those of water ( $\tilde{C}_{PF} = 75$  J/mol/K) and dodecane ( $\tilde{C}_{PS} = 375$  J/mol/K), respectively.<sup>113,114</sup> We approximate the membrane effective thermal conductivity to be that of air, 0.03 W/m/K.<sup>113</sup> The heat-transfer coefficient  $h$  is related to the mass-transfer coefficient through the Prandtl and Schmidt numbers (see Eq. C1 below)<sup>74</sup>

$$h = \frac{k_X k_m}{\bar{\rho} D} \left( \frac{Pr}{Sc} \right)^{1/2} \quad (\text{A22})$$

where the Prandtl number  $Pr = \nu/\alpha$  is the ratio of the fluid kinematic viscosity  $\nu$  to its thermal diffusivity  $\alpha$  and the Schmidt number  $Sc = \nu/D$  is the ratio of the kinematic viscosity to the diffusivity.  $Pr$  and  $Sc$  for feed water at 313 K are roughly 4 and 550,<sup>113</sup> respectively. Substitution of these values into Eqs. A18, A20, and A21 establishes that neither the solvent nor the feed temperature diverges from the inlet temperature by more than 0.2°C.

Figure A2 shows calculated temperature profiles for  $T_F$  and  $T_S$  as a function of axial position  $z$  (the cross-membrane temperature profile in the  $x$  direction in Figure A1 corresponds to  $z = 0$  in Figure A2). Energy loss due to feed vaporization and mass-transferred enthalpy cools the feed from  $T_{F0} = 40^\circ\text{C}$  at the inlet ( $z = 0$ ) to  $T_{FL} = 39.83^\circ\text{C}$  at the module exit ( $z = L$ ). Net total energy flux from feed to solvent heats the solvent from  $T_{SL} = 40^\circ\text{C}$  at its inlet ( $z = L$ ) to  $T_{S0} = 40.21^\circ\text{C}$  at its exit ( $z = 0$ ).

Temperature profiles in both Figures A1 and A2 are relatively insensitive to the partial-molar excess enthalpies. Even with excess enthalpies on the order of the enthalpies of vaporization (50 kJ/mol), temperature excursions remain less than 0.4°C. For the base-case scenario where  $F/S = 6$ , the quantity  $F\tilde{C}_{PF}/\tilde{S}\tilde{C}_{PS} - 1$  appearing in Eqs. A18–A21 is positive. However, for values of  $F/S < 5$ ,  $F\tilde{C}_{PF}/\tilde{S}\tilde{C}_{PS} < 1$ , yielding slightly different behavior of the temperature profiles. Nevertheless, sensitivity analysis of Eqs. A18, A20, and A21 reveals that  $T_S > T_F$  and temperature excursions within the MVE module remain less than a few tenths of degrees Celsius regardless of the magnitude of  $F\tilde{C}_{PF}/\tilde{S}\tilde{C}_{PS}$ .

Finally, we establish that the temperature maximum in the solvent and the temperature minimum at  $x = 0$  at the membrane upstream face (see Figure A1) do not depart far from the near-

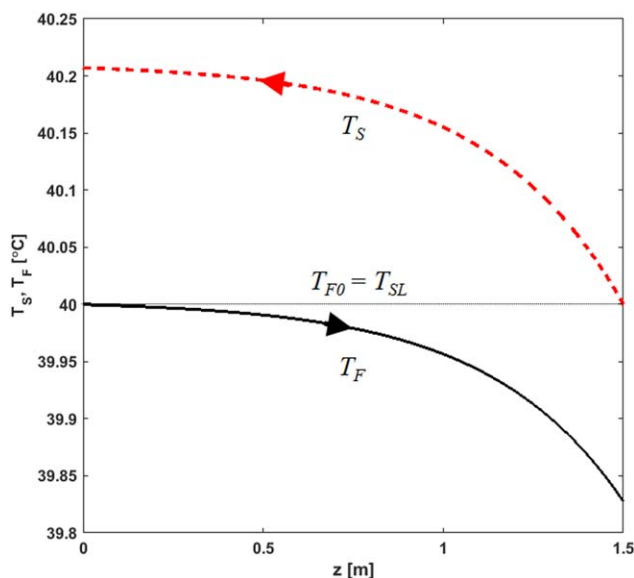


**Figure A2.** Temperature profiles for feed,  $T_F$  (solid line), and solvent,  $T_S$  (dashed line), as a function of axial position along the module,  $z$ . The horizontal dotted line indicates that both feed and solvent enter the module at  $T_{F0} = T_{SL} = 40^\circ\text{C}$ . Arrows point in direction of feed and solvent flows.

[Color figure can be viewed in the online issue, which is available at [wileyonlinelibrary.com](http://wileyonlinelibrary.com).]

isothermal feed and solvent streams. Equation A10 gives the temperature difference between the bulk feed and solvent streams and the corresponding membrane interfaces. These two temperature differences depend on the overall temperature difference between the two bulk streams, the heat-transfer coefficient, the molar fluxes, and the partial-molar excess enthalpies of butanol and water in the feed and solvent streams. Evaluation of Eq. A10 for base-case conditions yields a maximum feed and solvent temperature difference of 0.03°C. Accordingly, the maximum temperature excursion anywhere in the MVE module is at most a few tenths of degrees Celsius, validating an isothermal approximation. The dominant reason is the near cancellation of enthalpies of vaporization and dissolution at the two membrane faces. As a result, temperature variation of physical properties across the membrane, such as diffusivity, activity coefficient, density, and enthalpy, are negligible; although net energy is transferred from the feed to the solvent in an MVE unit, the net module heat demand is negligible.

## Appendix B : Membrane-Pore Concentration Profiles

To establish the cross-membrane species flux, the  $x$ -derivative of Eq. 1 is set to zero and the resulting ordinary differential equation is solved as

$$\frac{C_i(0) - C_i(x)}{C_i(0) - C_i(L_m)} = \frac{1 - \exp [Pe_m(x/L_m)]}{1 - \exp [Pe_m]} \quad (\text{B1})$$

Substitution of Eq. B1 into Eq. 1 gives Eq. 3 in the text.

## Appendix C : Feed and Solvent Mass-Transfer Coefficients

We utilize the Graetz–Lévéque analysis<sup>19,25,51,74,97,98</sup> for plug flow in a slit to predict the MVE unit channel mass-transfer coefficient  $k_X$ . Local Sherwood number,  $Sh_{loc}$ , in the channel-entrance region is a function of the local Graetz number,  $Gz_{loc}$ <sup>74</sup>

$$Sh_{loc} = \frac{1}{\sqrt{\pi}} Gz_{loc}^{1/2} \text{ for } z/L_e \leq 1 \quad (\text{C1})$$

and in the fully developed region,  $Sh_{loc}$  is given by<sup>74</sup>

$$Sh_{loc} = 4.935 \text{ for } z/L_e \geq 1 \quad (\text{C2})$$

where  $Sh_{loc} \equiv k_X \delta / (\bar{\rho} D)$ ,  $Gz_{loc} \equiv Pe(\delta/z)$ ,  $Pe \equiv \langle v \rangle \delta / D$  is the channel Péclet number, and  $z$  is the axial position along the flow channel.  $D$  is the binary diffusion coefficient of water (or butanol) in the feed or solvent flows. Likewise,  $\langle v \rangle$  and  $\bar{\rho}$  are the average velocity and molar density of the liquid feed and solvent streams, respectively. Finally,  $L_e = 0.065 Pe \delta$  is the flow-channel entrance length<sup>74</sup> of the MVE unit. For simplicity, we assume that Eqs. C1 and C2 hold for both feed and solvent streams.

We desire the length-averaged mass-transfer coefficient or Sherwood number obtained by integrating Eq. C1 over the entrance length, integrating Eq. A2 over the fully developed length, and dividing the sum of these two integrals by the total channel length,  $L$ . After integration and substitution of the expression for entrance length, we recover the length-averaged Sherwood number,  $Sh$ , as a function of average Graetz number,  $Gz$

$$Sh = \frac{k_X \delta}{\bar{\rho} D} = 0.129 Gz + 4.935 \text{ for } L_e/L \leq 1 \quad (\text{C3})$$

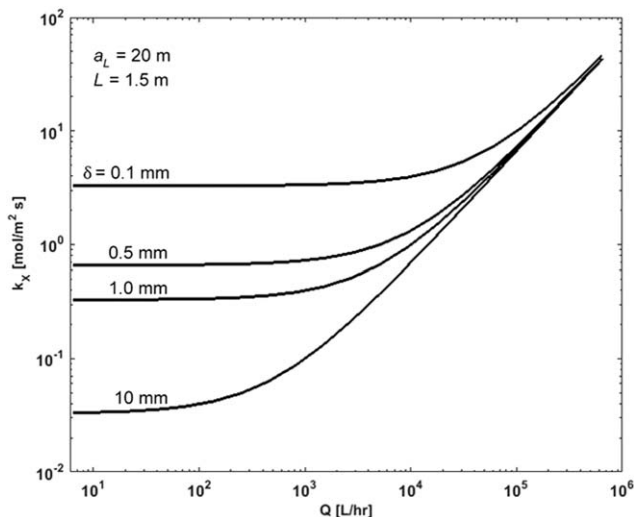


**Figure C1. Average mass-transfer coefficient from Graetz-Lévêque<sup>74,97,98</sup> for varying feed volumetric flow rates and spacer gap thickness.**

where the length-averaged Graetz number is given by  $Gz \equiv Pe(\delta/L)$ . The first term on the far right of Eq. C3 corresponds to the entrance region and the second term corresponds to the fully developed region of the channel. It proves convenient to rewrite Eq. C3 as

$$\frac{k_X}{\rho} = 0.258 \frac{Q}{a_L L} + 4.935 \frac{D}{\delta} \text{ for } L_e/L \leq 1 \quad (\text{C4})$$

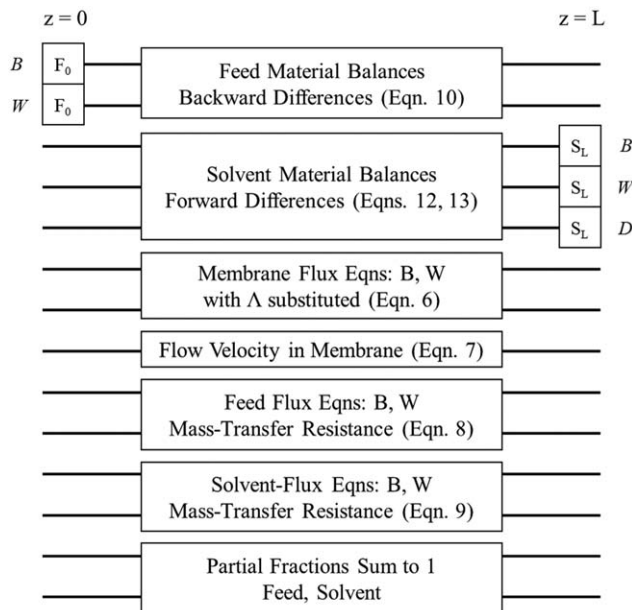
where  $Q = a_L \delta \langle v \rangle / 2$  is the feed (solvent) volumetric flow rate. Thus,  $k_X$  varies linearly with MVE volumetric (molar) flow rate. Equations C3 and C4 hold only when the entrance length is smaller than the channel length. Otherwise, Eq. C1 must be averaged over the channel length.

Figure C1 portrays illustrative mass-transfer coefficients as a function of MVE throughput in terms of volumetric flow rate for cases where there is a Lévêque entrance length. Typical volumetric throughputs of 100 L/h fall in the asymptotic region of low flow where the entrance length is short and does not contribute to mass transfer. Figure C1 accentuates the importance of channel-gap thickness in reducing mass-transfer resistance.

## Appendix D : Numerical Solution

Equations 5–11 are solved numerically using finite differences and a Newton–Raphson algorithm to resolve nonlinearities.<sup>98,115</sup> Details on the procedure and the BAND(j) subroutine implemented are available elsewhere.<sup>98,115</sup> For countercurrent flow, forward finite differences apply to the feed stream, whereas backward differences are written for the solvent stream. Figure D1 displays a BANDmap of the equations solved and the boundary conditions used.<sup>98,115</sup> Step size was reduced by increasing the number of nodes,  $n$ , until results were independent of meshing ( $n \sim 300$ ). Convergence was achieved for each variable when the residual sum of squares of all nodes was less than  $10^{-14}$ . All calculations were performed in MATLAB.

To incorporate the phase-equilibrium constraints, activity coefficients were calculated from NRTL and UNIFAC theories in subroutines outside of BAND. For simplicity, activity coefficients were held constant in converging Eqs. 5–11 and then changed by cyclic substitution in an outside loop. Convergence



**Figure D1. BANDmap for MVE-design model.**

of the outside loop was usually accomplished in less than five iterations.

## Appendix E : Entropy Production

Appendix A demonstrates that in the base-case MVE design, where both feed inlet and countercurrent solvent inlet flows are at 40°C, the feed stream cools while the solvent stream warms. Energy transfers from a lower temperature feed to a higher temperature solvent in seeming violation of required entropy production in irreversible processes. To establish that positive entropy is indeed produced in our MVE design, we invoke entropy balance per unit area across a local section of membrane at arbitrary axial position<sup>74</sup>

$$\sum_i N_i [\bar{S}_{iF}(0) - \bar{S}_{iS}(L_m)] + \frac{h_F [T_F - T_F(0)]}{T_F(0)} - \frac{h_S [T_S - T_S(L_m)]}{T_S(L_m)} + g_S L_m = 0 \quad (\text{E1})$$

where  $\bar{S}_{iF}(0)$  and  $\bar{S}_{iS}(L_m)$  are partial-molar entropies of the liquid feed stream and liquid solvent stream at the two membrane faces and  $N_i$  is the total diffusive and convected species molar flux (constant with respect to  $x$ ) at axial position  $z$ . Thus, the first term in Eq. E1 is the net convective influx of entropy into the membrane, and the second two terms give the thermal energy (heat) fluxes per unit temperature at the feed and solvent faces of the membrane.  $g_S$  is the net volume rate of entropy production in the membrane which must be positive.<sup>74</sup> We probe the sign of  $g_S$  by evaluating Eq. E1.

Substitution of Eq. A3 into the above result gives upon rearrangement

$$g_S L_m = \sum_i N_i \left\{ \left[ \bar{S}_{iS}(L_m) - \frac{\bar{H}_{iS}(L_m)}{T_S(L_m)} \right] - \left[ \bar{S}_{iF}(0) - \frac{\bar{H}_{iF}(0)}{T_F(0)} \right] \right\} + e_x \left[ \frac{1}{T_S(L_m)} - \frac{1}{T_F(0)} \right] \quad (\text{E2})$$

The chemical potential of species  $i$  relates partial-molar entropies and enthalpies according to  $\mu_i \equiv \bar{H}_i - T\bar{S}_i$ . Consequently, we rewrite Eq. E2 as

$$g_S L_m = \sum_i N_i \left[ \frac{\mu_{iF}(0)}{T_F(0)} - \frac{\mu_{iS}(L_m)}{T_S(L_m)} \right] + e_x \left[ \frac{1}{T_S(L_m)} - \frac{1}{T_F(0)} \right] \quad (\text{E3})$$

Entropy is produced in MVE when the right side of Eq. E3 is positive. Appendix A demonstrates that the total energy flux,  $e_x$ , is positive and that  $T_S(L_m) > T_F(0)$ . Consequently, the second term on the right of Eq. E3 is negative and corresponds to transfer of thermal energy against a temperature increase. However, the driving force for MVE separation is the difference in species chemical potentials between the feed and the solvent streams, specifically,  $\mu_{iF}(0) > \mu_{iS}(L_m)$ . Thus, as mass-transfer flux  $N_i$  is positive, the first term on the right of Eq. E3 is positive provided that  $T_F(0)$  and  $T_S(L_m)$  do not differ significantly. The algebraic sum of the two terms in Eq. E3 establishes the sign of entropy production in MVE.

To evaluate Eq. E3 quantitatively, we write the chemical potentials in the feed and solvent streams at the membrane faces as

$$\mu_{iF}(0) = \mu_i^o(0) + R_g T_F(0) \ln [\gamma_{iF}(0) X_{iF}(0)] \quad (\text{E4})$$

and

$$\mu_{iS}(L_m) = \mu_i^o(L_m) + R T_S(L_m) \ln [\gamma_{iS}(L_m) X_{iS}(L_m)] \quad (\text{E5})$$

where the superscript  $o$  indicates pure liquid species  $i$ . Next, we express the chemical potentials of the pure liquid species  $i$  per unit temperature in a Taylor series for small differences between  $T_F(0)$  and  $T_S(L_m)$  or

$$\begin{aligned} \frac{\mu_i^o(L_m)}{T_S(L_m)} &= \frac{\mu_i^o(0)}{T_F(0)} + \frac{d(\mu_i^o/T)}{dT} \Big|_{T_F(0), P} [T_S(L_m) - T_F(0)] + \dots \\ &= \frac{\mu_i^o(0)}{T_F(0)} - \frac{\tilde{H}_i^o(0)}{[T_F(0)]^2} [T_S(L_m) - T_F(0)] \end{aligned} \quad (\text{E6})$$

where the last term on the right utilizes the Gibbs–Helmholtz relation<sup>83</sup> and  $\tilde{H}_i^o$  is pure liquid molar enthalpy of species  $i$ . Recognition of the reference state  $\tilde{H}_i^o(0) = 0$ , consistent with Appendix A, along with substitution of Eqs. E4–E6 into Eq. E3 gives

$$g_S L_m = \sum_i N_i R_g \ln \frac{\gamma_{iF}(0) X_{iF}(0)}{\gamma_{iS}(L_m) X_{iS}(L_m)} + e_x \left[ \frac{1}{T_S(L_m)} - \frac{1}{T_F(0)} \right] \quad (\text{E7})$$

Species fluxes, activity coefficients, and compositions follow from the MVE-unit model in the text. Energy flux is conveniently calculated from Eqs. A3, A7, and A11. Finally, it is necessary to eliminate  $T_F(0)$  in favor of  $T_F$  and  $T_S(L_m)$  in favor of  $T_S$ .  $T_F(0)$  and  $T_S(L_m)$  are obtained from substitution of Eq. A10 into Eqs. A8 and A9, respectively.

Evaluation of Eq. E7 requires activity coefficients and compositions at  $x = 0$  and  $x = L_m$ . Values for  $X_{iF}$ ,  $X_{iS}$ , and  $N_i$  from the mass-transfer results in Figures 4 and 5 enable solution of Eqs. 7 and 8 for  $X_{iF}(0)$  and  $X_{iF}(L_m)$ , respectively. Activity coefficients in Eq. 7 are computed with the NRTL and UNIQUAC models<sup>82,83</sup> at the interface compositions. For temperatures, fluxes, and compositions exhibited in the base-case scenario,  $g_S L_m$  calculated with Eq. E7 varies between 0.002 and 0.7 W/m<sup>2</sup>/K along the unit. Thus, net entropy production is positive, satisfying the second law of thermodynamics.

A sensitivity analysis of Eq. E7 to partial-molar excess enthalpies and  $F/S$  confirms that entropy generation is positive. The first term on the right of Eq. E7 is positive and larger than the second. That is, the chemical-potential driving force of species  $i$  between the feed and solvent is positive, as required for a successful MVE separation process.

*Manuscript received Feb. 10, 2015, and revision received May 19, 2015.*